Available online at www.sciencedirect.com
ScienceDirect
Tetrahedron
Tetrahedron 63 (2007) 3491–3514

The spectroscopy, dynamics, and electronic structure of pyrenyl–dU nucleosides: $P^{\bullet+}/dU^{\bullet-}$ charge transfer state photophysics

Thomas L. Netzel*

Department of Chemistry, Georgia State University, PO Box 4098, Atlanta, GA 30332-4098, United States

Received 3 August 2006; revised 7 November 2006; accepted 7 November 2006
Available online 2 February 2007

Abstract—Various spectroscopies including UV–vis absorbance, emission, and emission quantum yield are combined with a variety of kinetics measurements including time resolved emission and nanosecond, picosecond, and femtosecond transient absorbance (TA) to systematize the $P^{\bullet+}/dU^{\bullet-}$ charge transfer (CT) state dynamics of a variety of pyrenyl–dU nucleoside conjugates in several solvents of varying polarity. These results are then analyzed further by means of electronic structure computations in vacuum and using two different solvent models. Finally, the excess electron dynamics of a number of DNA duplex structures substituted with two different pyrenyl–dU nucleosides and 5-XdU, where X=Br or F, electron traps are discussed in terms of achieving high yields of long-lived photoinduced CT products in DNA.

1. Introduction

One of the most exciting aspects of the study of covalently labeled DNA nucleosides, duplexes, and hairpins is the increasing use of electronic structure and molecular dynamics (MD) calculations, including their combined use, to provide detailed insights into the excited state structures and dynamics of these systems.[1–5] Control of the emission and photoinduced charge transfer (CT) state lifetimes of these labeled DNA assemblies is of significant practical interest, and increasingly computations are proving useful in understanding how to do this. However, my collaborators and I began synthesizing covalently labeled uridine and cytidine nucleosides in the late 1980s before such computations became as powerful and accessible as they are today.[6] Prior to our entry into this field, Dreyer and Dervan had attached a seven-atom linker terminating in a primary amine to C5 of uracil.[7] This modified uridine was then reacted with Fe–EDTA for DNA footprinting studies. Much of our work in the intervening years has continued to attach linkers to this same C5 site. However, as time progressed we concentrated our work on short, one-to-three atom length linkers to control the location of attached labels in the major groove of the labeled DNA duplex. Also prior to our entry into this field, Gillam and Tener employed a transamination reaction between cytidine and 1,6-diaminohexane to create a labeled cytidine with an eight-atom linker attached to N^4.[8] They then biotinylated this nucleoside conjugate for use in enzymatic detection assays.

In our initial work the octameric base sequence 5′-GCACT CAG-3′ was studied and either the central C or T site was modified with a linker terminating in a primary amine. This amine was in turn reacted with a variety of labels: pyrenesulfonyl, pyrenebutyrate, biotin, and fluorescein.[6] Duplexes formed from oligomers with a labeled U (in place of T) showed normal melting behavior while those formed with a labeled C did not. In the U-labeled duplexes, fluorescein emission was quenched a factor of six relative to the label itself; pyrenesulfonyl emission was quenched a factor of 12; and pyrenebutyrate emission was quenched a factor of 500. This work showed that chemically modified bases and standard solid state synthesis protocols could be used to make DNA oligomers and duplexes selectively labeled at internal sites. While it was speculated in this work that intramolecular CT between DNA bases and the photoexcited labels may have been responsible for the extensive emission quenching other studies were needed to confirm this possibility.

Generally organic labels were attached to DNA oligomers. One of the first studies to attach metalloporphyrins to oligomers was carried out by Helene and co-workers.[9] The attachment points in this work and in many others were at the 3′ or 5′ terminal phosphates. As note above Dreyer and Dervan had attached an inorganic coordination complex, Fe–EDTA,

Keywords: Transient absorbance spectroscopy; Laser kinetics; Time resolved emission; Charge transfer excited states; DNA duplexes; Pyrene; Pyrenyl–dU; Pyrenyl nucleoside conjugates; DNA hairpins; INDO; CIS; DRF; SCRF; Solvent conformational heterogeneity; Solute conformational heterogeneity; Calculated emission spectra; Calculated absorption spectra; Solvent molecular dynamics.
* Tel./fax: +1 404 651 3129; e-mail: tnetzel@gsu.edu

0040–4020/$ - see front matter © 2007 Elsevier Ltd. All rights reserved.
doi:10.1016/j.tet.2006.11.095

to a modified internal base in an oligomer.[7] We extended this latter work by incorporating a fluorescent as well as redox-active inorganic label to an internal base; the label was a derivative of tris(2,2′-bipyridine)ruthenium(II) ($Ru(bpy)_3^{2+}$).[10] Again either a central C or T site was modified in octamers with the same 5′-GCACTCAG-3′ sequence. The linker was eight atoms long for addition of bipyridine to C5 of uracil and six atoms long for addition to N^4 of the cytosine. In contrast to the fluorescence behavior of the above organic fluorophores, ruthenium emission yields from covalently attached $Ru(bpy)_3^{2+}$ labels, in short DNA duplexes were identical to that of $Ru(bpy)_3^{2+}$ itself in the same buffer solution. The fact that covalent attachment of $Ru(bpy)_3^{2+}$ to DNA duplexes caused neither emission quenching nor enhancement for either U or C modes of attachment was consistent with an earlier report that exogenous $Ru(bpy)_3^{2+}$ did not associate with duplex DNA.[11] Neither mode of Ru-labeling caused appreciable duplex destabilization relative to the corresponding unmodified duplex.

An interesting attempt to label doubly DNA duplexes and thereby to induce label/label interactions, either excimer formation or CT emission quenching, in preference to label/duplex interactions involved the use of pairs of pyrenebutyrate and pyrenesulfonate and mixed pairs of pyrene/anthraquinone labels attached via eight-atom linkers to a central T site (i.e., at C5 uracil) in each strand of a duplex based on the 5′-GCACTCAG-3′ sequence and its complement.[12] DNA melting studies of these duplexes showed that both the pyrenebutyrate and anthraquinone labels stabilized duplexes by 1.5 kcal/mol per label relative to the corresponding duplexes modified only with terminal amines (i.e., lacking pyrenyl or anthraquinone labels). In contrast a single pyrenesulfonate label had the same free energy of duplex formation as the corresponding duplex with only a terminal amine linker. Not surprisingly under these circumstances label/duplex interactions dominated label/label interactions for duplexes with pyrenebutyrate, mixed pyrenebutyrate/anthraquinone, and mixed pyrenesulfonate/anthraquinone pairs of ligands. The single instance of label/label interactions dominating label/duplex ones occurred for the duplex with two pyrenesulfonate labels. In this case, the emission quantum yield was one-third lower for the latter duplex compared to one with a single pyrenesulfonate label. Additionally, each of the three emission lifetime components measured was significantly shortened in the case of two labels compared to only one label. Excimer emission was not seen from the duplex with two pyrenesulfonate labels, however, most likely due to CT quenching of excimers by neighboring DNA bases. The reactivity of a 5′-phosphate linked pyrenyl label toward bases in the attached duplex was confirmed subsequently.[13] In that work 96% of the pyrenyl label's emission was quenched compared to an identical concentration of free 4-(1-pyrenyl)butanol. Clearly, DNA bases are too reactive toward pyrenyl excited singlet states to use long flexible linkers if the goal is to direct excited state reactivity along specific channels. Ways of reducing label/duplex interactions include using shorter linkers to join bases and labels and also introducing redox-inactive 'blocking' groups on neighboring nucleotides to prevent excited labels from contacting DNA bases. The remainder of this paper will explore these ideas in greater detail.

2. Results and discussion

2.1. Demonstrations of CT quenching of photoexcited pyrene by DNA bases

2.1.1. Pyrenyl-dG. Geacintov and co-workers[14–17] examined photoinduced CT mechanisms in the covalently linked pyrenyl-dG adduct a shown in Figure 1 and in mixtures of 7,8,9,10-tetrahydroxytetrahydrobenzo{*a*}pyrene (BPT) with dG.[15] In polar organic solvents, pyrenyl radical anions ($BPT^{\bullet-}$) were observed in solutions of BPT and dG (0.1 M). Radical ions were not seen in either the covalent adduct (+)-*trans*-BPDE-N^2-dG or in aqueous solutions of BPT and dG on timescales >10 ns. However, in these latter systems the primary products of fluorescence quenching were pyrenyl triplet excited states with greatly enhanced yields (3–10 fold larger than expected from normal intersystem crossing). The mechanism of enhanced triplet yield involves photoinduced CT from dG to pyrenyl residues, followed by rapid and efficient charge recombination to form pyrenyl triplet excited states. A follow-on study with higher time resolution showed that the rate of charge separation within (+)-*trans*-BPDE-N^2-dG in *N*,*N*′-dimethyl formamide (DMF) was 110 ps and the rate of charge recombination was 560 ps resulting in a CT efficiency of 0.8±0.2. In hydrogen bonding solvents such as *N*-methylformamide (NMF) and formamide (FA) the rates of CT from dG to BPDE decreased, while the rates of charge recombination increased. The overall result was that the yields of radical ions were less than 0.15 in the hydrogen bonding solvents. In aqueous solutions of the adduct, the rate of CT slowed even further, and radical ion products were not observed, presumably due to very rapid charge recombination. Interestingly, a kinetic isotope solvent effect (k_H/k_D) of 1.5 suggests that solvent H-bonds influence the intramolecular CT rates in (+)-*trans*-BPDE-N^2-dG.[17] Relatedly, Wagenknecht and co-workers have recently reported studying the fluorescence properties of the $P^{\bullet-}/dG^{\bullet+}$ CT state in DNA single strands and duplexes

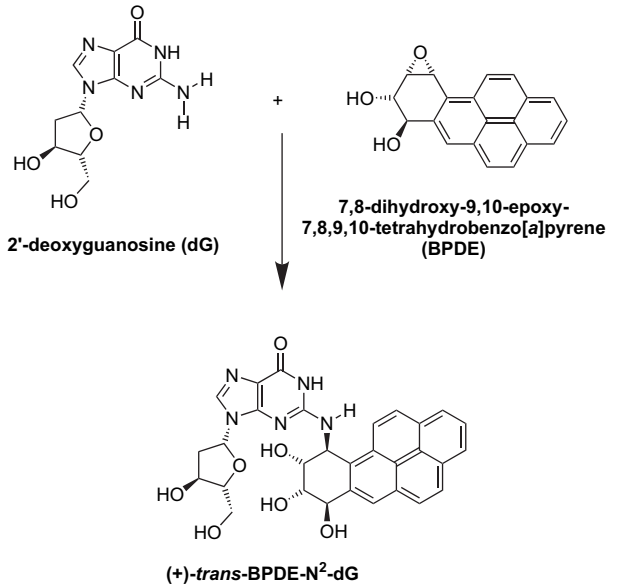

Figure 1. Reaction of carcinogenic and mutagenic BPDE with the exocyclic amino group of dG to form the (+)-*trans*-BPDE-N^2-dG adduct.

labeled with 8-(pyren-1-yl)-2′-deoxyguanosine (PdG) in which pyrene is directly bonded to C8 of dG.[18] They found up to 25-fold enhanced CT state emission in duplexes compared to single stands.

In 1995 Geacintov and co-workers examined the fluorescence quenching of BPT by the 2′-deoxynucleosides dG, dC, and dT.[16] In the case of dC and dT, the thermodynamics of CT are favorable in water, and fluorescence quenching exhibits a solvent kinetic isotope effect; however, in the polar organic solvent dimethylsulfoxide (DMSO) they did not observe fluorescence quenching. Importantly, $\leq$10 ns after laser excitation of aqueous mixtures of BPT with dC and dT prominent transient absorption maxima were seen at 455 nm indicating the formation of $BPT^{\bullet+}$ radical cations. Thus for BPT with dC and dT in water, CT from the pyrenyl singlet excited state proceeded from pyrenyl residue to DNA base; in contrast for BPT with dG in polar organic solvents and reasonably also in water, CT from the same excited state proceeded from DNA base to pyrenyl residue. Interestingly, the reduction potential (vs SCE) varied upon protonation from −2.5 V for $dC/dC^{\bullet-}$ in DMF to −1.3 V for $dC/dC(H)^{\bullet}$ in water and from −2.4 V for $dT/dT^{\bullet-}$ in DMF to −1.3 V for $dT/dT(H)^{\bullet}$ also in water.[16] Corresponding reduction potential increases relative to their values in DMF for solvent H-bonding are not known.

2.1.2. P12dU. Also in 1995 Netzel and co-workers published a series of papers exploring the photophysics of pyrene labeled nucleosides, oligonucleotides, and duplexes.[19–21] Emission from pyrenebutanoic acid (PBA) in methanol (MeOH) is characterized by a sharp electronic origin band at 376 nm and two distinct vibrational bands of decreasing intensity at 396 and 416 nm with no emission beyond 465 nm.[20] Emission from P12dU (see Fig. 2 for the structure of this nucleoside) in the same solvent has nearly identical spectral features to those of pyrene but also emits appreciably at 495 nm. Table 1 lists the emission lifetimes for these two compounds in MeOH. The emission kinetics for P12dU is considerably more complicated than for PBA. At 400 nm three lifetime components are required to fit the nucleoside's emission, while four components are required at 495 nm. The latter emission arises from a $P^{\bullet+}/dU^{\bullet-}$ CT state formed by electron transfer quenching of the initially formed pyrenyl (π,π*) state. Note that the pyrenyl (π,π*) emission at 400 nm lasts only for 38 ns in the nucleoside but lasts as long as 231 ns in PBA. The CT emission increases with an 18-ns lifetime and lives much longer than the (π,π*) emission (51 ns vs 38 ns). The 12-ns (π,π*) emission lifetime component at 400 nm lies between the 2.7 and 18 ns CT components at 495 nm and could be replaced by them with equally good fitting consequences. Clearly the CT and (π,π*) states are distinct and not in equilibrium.

Based on free energy estimates for CT quenching of pyrenyl (π,π*) states by DNA nucleosides, dA should quench the slowest, dG more rapidly, and dT and dC the most rapidly and at roughly the same rate. Note that CT quenching is expected to be reductive for dA and dG as they are both electron rich, but oxidative for dT and dC as they are both electron poor. Table 2 lists the emission lifetimes for four pentameric nucleotides each with a central P12dU subunit (dU*): each pentamer as the base sequence XXdU*XX, where X=dA, dG, dT, and dC. One of the first observations is that two of the emission lifetimes for $dA_2dU^*dA_2$ in buffer at 400 nm are much longer that those of the P12dU nucleoside in MeOH at the same wavelength. Additionally, CT emission is extremely weak for this pentamer. The conclusion is that the flanking dA nucleotides inhibit CT quenching of pyrenyl emission by dU*. For the $dG_2dU^*dG_2$ pentamer, both CT and pyrenyl emission are seen with an average pyrenyl emission lifetime at 400 nm of 8.3 ns compared to 40 ns for $dA_2dU^*dA_2$. Excepting the 0.03 amplitude 20-ns component for $dT_2dU^*dT_2$, both $dT_2dU^*dT_2$ and $dC_2dU^*dC_2$ have similar pyrenyl quenching behavior at 400 nm with average

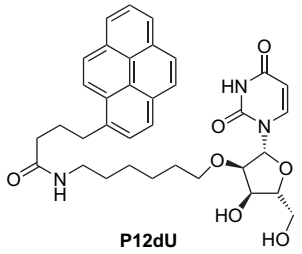

Figure 2. Structural drawing of the P12dU nucleoside used for internal substitution in DNA oligomers and duplexes.

Table 1. Emission lifetime (ns) data for PBA and P12dU in MeOH[a]

Molecule	400 nm	495 nm
PBA	125 (0.45) 231 (0.55)	
P12dU	0.6 (0.39) 12 (0.16) 38 (0.45)	0.4 (0.63) 2.7 (0.06) 18 (−0.18)[b] 51 (0.31)

[a] Lifetime component (relative amplitude). Data obtained from Ref. 19.
[b] Negative emission lifetime amplitudes indicate an increase (or growth) in emission intensity.

Table 2. Emission lifetimes (ns) for four dU*-labeled polynucleotides in buffer[a]

Polynucleotide	400 nm[b]	495 nm[b]
$dA_2dU^*dA_2$	5.9 (0.26) 30 (0.38) 64 (0.33) 200 (0.03)	Only trace emission
Average lifetime	40 ns	
$dG_2dU^*dG_2$	1.7 (0.58) 8.3 (0.28) 30 (0.13) 108 (0.01)	0.7 (0.40) 10. (0.28) 33 (0.20) 63 (0.12)
Average lifetime	8.3 ns	
$dT_2dU^*dT_2$	0.2 (0.81) 1.5 (0.09) 5.3 (0.07) 20 (0.03)	0.1 (0.79) 1.3 (0.16) 6.8 (0.05)
Average lifetime	1.3 ns	
$dC_2dU^*dC_2$	0.14 (0.71) 1.3 (0.25) 5.6 (0.04)	Only trace emission
Average lifetime	0.6 ns	

[a] dU* is nucleotide form of the P12dU nucleoside. Data obtained from Ref. 19.
[b] Lifetime component (relative amplitude).

emission lifetimes of about 1 ns. In contrast, charge recombination within the $P^{\bullet+}/dC^{\bullet-}$ and $P^{\bullet+}/dU^{\bullet-}$ CT products in $dC_2dU^*dC_2$ appears to be much faster than within the same products in $dT_2dU^*dT_2$. The pyrenyl (π,π^*) emission quenching results for the four pentamers in Table 2 thus agree well with the relative CT quenching rates expected for dA, dG, dT, and dC nucleotides flanking dU*.

2.1.3. PdU. Figure 3 shows the structures of four pyrenyl–dU nucleoside conjugates with zero, one, two, and three linking atoms. Figure 4 presents absorption and emission spectra for the PdU nucleoside with no linking atoms in nonpolar tetrahydrofuran (THF) and in polar methanol (MeOH).[20] In contrast to PBA and P12dU, none of the absorption or emission spectra for PdU show vibrational structure, rather only weak vibrational shoulders are present in absorption but not in emission spectra. In THF PdU has an emission quantum yield of 0.42, but only 0.027 in MeOH. The broad emission from PdU in MeOH originates mostly from the $P^{\bullet+}/dU^{\bullet-}$ CT state. The emission lifetimes observed in the 400–560 nm range show important lifetime variations with wavelength. A small (0.01–0.05) amplitude emission decay decreases monotonically from 3.2 ns (400 nm) to 1.9 ns (520 nm) and then is absent at 560 nm. Most likely this emission component arises from PdU conformers that have the slowest pyrenyl (π,π^*) CT quenching lifetimes. Most PdU conformers form the $P^{\bullet+}/dU^{\bullet-}$ CT state in ca. 50 ps or less as evidenced by the large amplitude (0.9–0.7) emission decays that occur with this lifetime from 400 to 520 nm. The amplitude of this ultrafast emission component decreases with increasing wavelength as expected for pyrenyl (π,π^*) emission. In accord with a model of dual state emission, the amplitude of the middle emission lifetime component in the 400–520 nm range ca. 0.9 ns increases from 0.09 to 0.28 with increasing wavelength. Finally, at 560 nm, where the pyrenyl (π,π^*) state no longer emits, only two emission lifetimes are seen: 120 ps (0.46 amplitude) and 0.91 ns (0.54).[20] The changing distribution of emission lifetimes and amplitudes with variation of wavelength indicates formation of an initial pyrenyl (π,π^*) state followed by formation of a $P^{\bullet+}/dU^{\bullet-}$ CT state that is not in equilibrium with the initial pyrenyl state. Additionally, different PdU conformers form the CT state with lifetimes ranging from $\leq$50 ps to 3.2 ns.

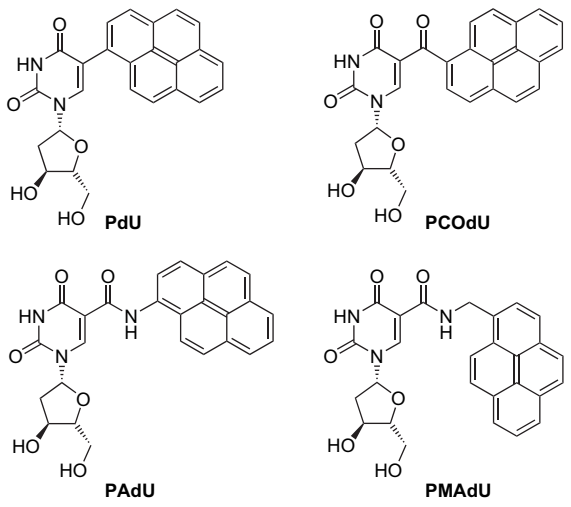

Figure 3. Structural drawings of four pyrenyl–dU nucleoside conjugates with, respectively, zero (PdU), one (PCOdU), two (PAdU), and three (PMAdU) linking atoms.

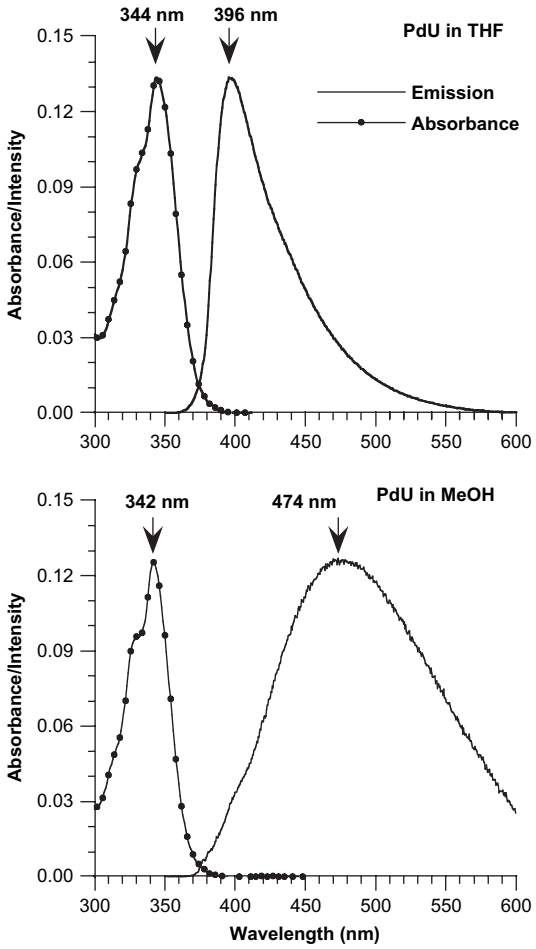

Figure 4. Plots of absorbance versus wavelength and normalized, corrected emission intensity versus wavelength for PdU in THF (top) and MeOH (bottom). Adapted with permission from the Journal of the American Chemical Society.[20] Copyright 1995 American Chemical Society.

For PdU in THF and acetonitrile (MeCN), CT and pyrenyl (π,π^*) emission appear 'blended', and the emission quantum yields are, respectively, 16-fold and 13-fold larger than in MeOH (see Table 3). In keeping with the blended emission model, the emission lifetimes in the 395–495 nm range in both solvents exhibit nearly the same dual decay lifetimes at all wavelengths: subnanosecond (up to 0.36 amplitude in MeCN and 0.24 in THF) and 6–7 ns.[20,21] The two lifetimes likely arise from population equilibration for the pyrenyl (π,π^*) and $P^{\bullet+}/dU^{\bullet-}$ CT states at short time followed by 6–7 ns decay of these equilibrated states.

Table 3. Emission quantum yields ($\phi_{em}\times10^3$) for four pyrenyl–dU nucleosides in three solvents[a]

Nucleoside	THF	MeCN	MeOH
PdU	420	350	27
PCOdU	28	5	2
PMAdU	16	1.1	5.6
PAdU	1.8	0.97	0.075

[a] Data obtained from Refs. 20,29,31.

Importantly, no pyrenyl emission lifetime components distinct from CT emission ones, especially at long times, are seen in THF and MeCN in contrast to P12dU and PdU in MeOH and the XXdU*XX pentamers in buffer.

In 2004 Fiebig and co-workers[22] studied the photophysics of PdU in MeCN and water. In water at pH 11 where the CT state could not be protonated, a blended emission spectrum was observed nearly identical to that seen for PdU in THF. Judging from their reported emission spectra, the emission quantum yield in water at pH 11 appears to be half of that in MeCN (quantum yields were not reported). In water at pH 5, where the $P^{\bullet+}/dU(H)^{\bullet}$ photoproduct could be formed, the pyrenyl (π,π^*) state was quenched in 4.7 ps and the separated charges in $P^{\bullet+}/dU(H)^{\bullet}$ recombined in 110 ps. The very low energy of the protonated photoproduct was responsible for its short lifetime and low emission intensity. The puzzling question is why do the emission properties (i.e., its spectrum and apparent quantum yield) of PdU in water at high pH resemble so closely to those of PdU in solvents like THF and MeCN where PdU exhibits blended emission kinetics, rather than those of PdU in the H-bond donating solvent MeOH where formation of an initial pyrenyl (π,π^*) state is followed by formation of a $P^{\bullet+}/dU^{\bullet-}$ CT state that is not in equilibrium with the initial pyrenyl state. Might this be a hydrophobic effect?

Importantly, Fiebig and co-workers[23] also inserted PdU into duplex DNA with and without nearby 5-bromo-2′-dexoyuridine (U^{Br}) excess electron traps. They provided both femtosecond kinetics and strand-cleavage evidence that a portion of the initially produced $P^{\bullet+}/dU^{\bullet-}$ CT state undergoes secondary electron transfer to nearby U^{Br} sites. No estimate of the quantum yield for this latter process was provided. It is also noteworthy that Mayer-Enthart and Wagenknecht[24] have successfully incorporated five adjacent PdU nucleotides into the central portion of a 19 base-pair DNA duplex. This latter duplex showed a strong CD signal in the pyrenyl region that was absent in a corresponding duplex with only a single central PdU substitution. The implication is that the five adjacent pyrenyl chromophores formed a helical π-stack outside the DNA duplex. This novel result supports the idea of using a DNA helix as a structural scaffold and has high potential for use in fluorescent DNA assays such as base-mismatch detection.

2.1.4. 2′-*O*-(1-Pyrenylmethyl)uridine (PMeU). The PMeU nucleoside is perhaps similar to PdU in that both have pyrenyl chromophores that are closely connected to the nucleoside core, but still maintain the normal sugar and base structures. In PMeU the pyrenyl chromophore is joined to the 2′-O of the sugar via a methyl group. Yamana and coworkers[25–27] showed that in an internally substituted DNA duplex the pyrenyl group was intercalated into the duplex, whereas in a similar RNA duplex the pyrenyl chromophore was located outside the duplex. As was seen above for multiple adjacent PdU nucleosides in a DNA duplex, Nakamura and Yamana[28] report formation of a helical π-stack of adjacent pyrenes in a 19 base-pair RNA duplex with up to four internally substituted PMeU nucleosides. As the number of PMeU substitutions increased, the pyrenyl CD absorption signal strengthened and pyrenyl excimer fluorescence increased strongly.

2.1.5. PCOdU. For PCOdU in MeOH, the emission spectrum is almost identical to the blended one seen for PdU in THF, but the emission quantum yields (ϕ_{em}) are very different: 0.002 for the former and 0.42 for the latter.[20] In contrast to their different ϕ_{em} values, both PCOdU in MeOH and PdU in THF show similar dual decay emission lifetimes: for PCOdU in THF at all wavelengths in the 382–450 nm range ca. 0.5 ns (0.3 amplitude) and 8.6 ns (0.7). The CO linker attached to both pyrenyl and uracil subunits could be argued both to make pyrene harder to oxidize and uracil easier to reduce, thus possibly canceling out redox changes to the energy of a $P^{\bullet+}/dU^{\bullet-}$ CT state relative to its energy in PdU. However, the much lower ϕ_{em} values for PCOdU in THF, MeCN, and MeOH compared to those for PdU in the corresponding solvents as seen in Table 3 suggest that the net effect of the CO linker is to make uracil in PCOdU easier to reduce than in PdU. Transient absorbance (TA) measurements on PCOdU in MeOH discussed below demonstrate that emission spectrum is due to a small minority of conformers that undergo CT quenching of their pyrenyl (π,π^*) states relatively slowly (ca. 8.6 ns).

In THF PCOdU has an emission spectrum that shows well resolved C–C vibrational bands at 387, 406, and 428 nm as expected for pyrenyl (π,π^*) emission. The emission kinetics for PCOdU in THF are complicated, requiring four decay lifetimes for good fits throughout the 382–450 nm range: $\approx$1.0 ns (0.3 amplitude), 8 ns (0.6), 15 ns (0.08), and 94 ns (0.02).[20] Given that the $P^{\bullet+}/dU^{\bullet-}$ CT state is in equilibrium with the pyrenyl (π,π^*) state for PdU in THF and that the same CT state in the same solvent is a much more effective quencher of pyrenyl emission in PCOdU than in PdU, it is reasonable to conclude that for PCOdU in THF the CT state is lower in energy than the pyrenyl local excited (LE) state. If so, the nearly pure pyrenyl emission with sharp C–C vibrational bands must arise from a minority of PCOdU conformers that undergo pyrenyl emission quenching with a wide variety of lifetimes in the range $\approx$1.0–94 ns. This interpretation of the emission spectra for PCOdU in THF and MeOH implicitly suggests that at very short times the majority of nucleoside conformers have $P^{\bullet+}/dU^{\bullet-}$ CT states with energies well below the energy of the pyrenyl (π,π^*) state, but that in both solvents a minority of conformers do not. Furthermore the 'blended' emission spectrum for PCOdU in MeOH and the vibrationally resolved emission spectrum for the same nucleoside in THF suggest that the minority conformers have CT/pyrenyl equilibrated (or exciplex) excited states in MeOH and pure pyrenyl (π,π^*) states in THF. This is consistent with less CT stabilization (or higher energy CT states) in THF compared to MeOH. Taken as a whole these emission quantum yield, spectral, and lifetime results for PdU and PCOdU demonstrate that the combination of pyrenyl substitution and change of solvent polarity varies the energy of their $P^{\bullet+}/dU^{\bullet-}$ CT states relative to the energy of their pyrenyl (π,π^*) states.

Figure 5 is important for understanding why ϕ_{em} for PCOdU in MeOH is only 0.002, while it is 0.42 for PdU in THF and yet both nucleosides have similar blended emission spectra. Clearly if the CT and pyrenyl (π,π^*) states were equilibrated for PCOdU in MeOH, one would expect a larger emission quantum yield than 0.002. Figure 5 shows plots of TA

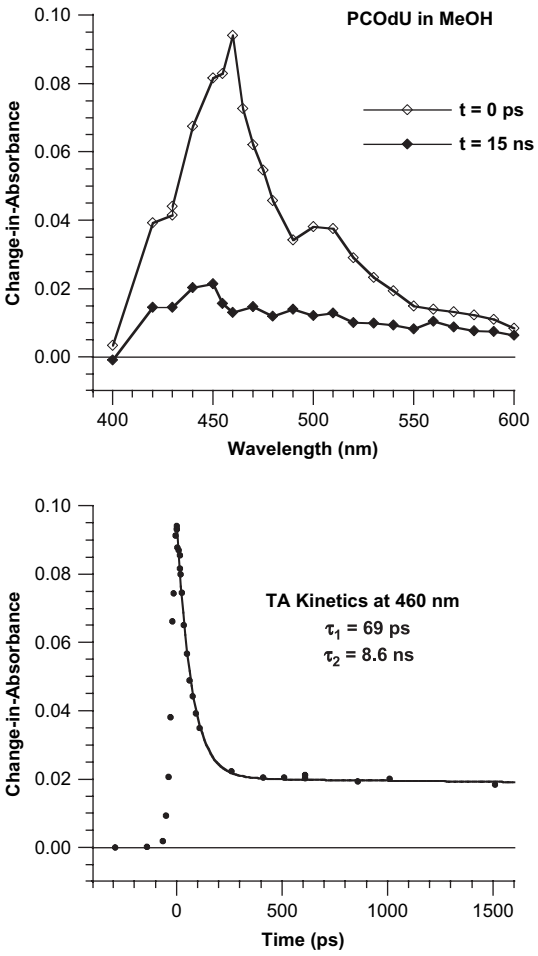

Figure 5. Top: Picosecond transient absorption (TA) spectra for PCOdU in MeOH immediately (t=0 ps) and 15 ns after photoexcitation at 355 nm (FWHM~25 ps). Bottom: TA kinetics data (solid circles) at 460 nm in the −300–500 ps time range fit (solid line) to 69-ps and 8.6-ns exponential decay lifetimes with an asymptote of 0.014 (R=0.9985). Reprinted in part with permission from the Journal of Physical Chemistry.[21] Copyright 1995 American Chemical Society. The kinetics data were reanalyzed for this figure.

spectra at 0 ps and 15 ns and TA kinetics at 460 nm for PCOdU in MeOH. The 0-ps spectrum shows that a strong, sharp absorption maximum at 460 nm with a broad shoulder (490–550 nm) is formed within the 30-ps excitation period. This absorption increase is characteristic of the pyrenyl$^{\bullet+}$ cation radical and shows that the P$^{\bullet+}$/dU$^{\bullet-}$ CT state is formed in $\leq$30 ps. Its large amplitude suggests that most PCOdU conformers charge transfer in this time range. However, the earlier discussed emission lifetime results for this system show that some conformers have a pyrenyl $^1(\pi,\pi^*)$ emission lifetime as long as 8.6 ns. The asymptote in the kinetics fit at 460 nm is consistent pyrenyl triplet states being formed via either CT or pyrenyl singlet relaxation. Indeed the 15-ns TA spectrum shows stronger absorption in the 420–450 nm range (where the pyrenyl $^3(\pi,\pi^*)$ state absorbs strongly) than in the 480–500 nm range (where the pyrenyl $^1(\pi,\pi^*)$ state absorbs strongly). The short, 69-ps lifetime of the P$^{\bullet+}$/dU$^{\bullet-}$ CT state explains why the emission quantum yield for PCOdU is so low in MeOH: the vast majority of photoexcited PdU conformers undergo CT in $\leq$30 ps and then decay in 69 ps. A minority of photoexcited PCOdU conformers emits as long 8.6 ns and is responsible for the observed 'blended' emission spectrum. Two cases of blended emission then appear to occur: for PdU in THF the emission quantum yield is high and is consistent with an equilibrium between the pyrenyl $^1(\pi,\pi^*)$ and CT states for most if not all nucleoside conformers, while for PCOdU in MeOH the emission quantum yield is very low due to fast CT state formation and relaxation for most nucleoside conformers with a minority of conformers producing blended emission with an 8.6-ns lifetime. In both cases biexponential emission decays are seen throughout the pyrenyl emission region and the longest lifetime components in the two cases are comparable, 6.4 ns for PdU in THF and 8.6 ns for PCOdU in MeOH.

2.1.6. PAdU. As expected based on the above discussion of increased pyrenyl emission quenching for PdU and PCOdU due to increased stabilization of the P$^{\bullet+}$/dU$^{\bullet-}$ CT state (or product) in the solvent series THF, MeCN, and MeOH, a similar solvent dependent decrease in ϕ_{em} is seen in Table 3 in the same series for PAdU, respectively, 1.8×10^{-3}, 0.97×10^{-3}, and 0.075×10^{-3}.[29] These emission yields correspond to emission quenchings relative to the *N*-acetyl-1-aminopyrenyl model (PAAc, i.e. PAdU with a methyl group in place of dU) in the corresponding solvent of 95%, 96%, and 99%, respectively. Alternately expressed, the emission yield is reduced 24-fold on going from THF to MeOH and 13-fold on going from MeCN to MeOH. It is striking to note in Table 3 that the corresponding emission yields for PAdU in this solvent series are much lower than those for either PdU or PCOdU. Clearly, the CT state is much lower in energy in PAdU than in the other two nucleoside conjugates. Attaching the amino group to pyrene in PAdU makes pyrene easier to oxidize than pyrene in either PdU or PCOdU. This conclusion is supported by PM3 calculations that show the HOMO energy in (*N*-methyl)-1-aminopyrene to be 0.2 eV higher in energy than in 1-methylpyrene.[29]

Figure 6 shows normalized emission spectra for PAdU in the above three solvents. Two aspects of these spectra stand out: (1) in THF and MeCN they appear to be 'blended' emission and (2) sharp vibrational bands are seen in MeOH. For example, the spectrum of PAdU in MeOH looks similar to

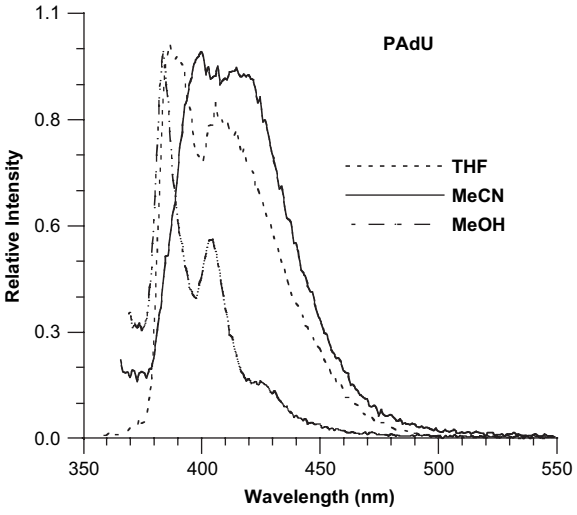

Figure 6. Normalized, corrected emission spectra for PAdU in THF, MeCN, and MeOH. Adapted with permission from the Journal of Physical Chemistry B.[29] Copyright 2000 American Chemical Society.

that for PCOdU in THF discussed above. Strikingly, ϕ_{em} in the latter case is 28×10^{-3} and in the former it is 0.075×10^{-3} (see Table 3), giving a ϕ_{em} ratio of 370. Based on the above discussion for PCOdU and the very small emission quantum yields seen for PAdU, it is reasonable to expect the PAdU emission spectra to be dominated by nucleoside conformers that are 'slow' to form $P^{\bullet+}/dU^{\bullet-}$ CT states. But how fast is CT quenching in the majority of conformers, and how long do their CT states live? Figure 7 presents femtosecond TA spectra for PAdU in MeCN (they are remarkably similar in MeOH).[30] The TA kinetics yield decay lifetimes in MeCN of 5.3±0.2 ps and 2.7±1.5 ns and in MeOH of 6.0±1.1 ps and 2.5±1.5 ns. Importantly, the $P^{\bullet+}/dU^{\bullet-}$ CT state is formed in the vast majority of PAdU conformers within 600 fs of photoexcitation. Thus the TA kinetics for PAdU in MeCN (see Fig. 7) and MeOH tell a story that is similar to that for PCOdU in MeOH in Figure 5 with the quantitative difference that the $P^{\bullet+}/dU^{\bullet-}$ CT product lives for 5–6 ps for PAdU in the two polar solvents and for 69 ps for PCOdU in MeOH. For both compounds the ns-lived, second decay components correspond to pyrenyl $^1(\pi,\pi^*)$ states in a minority of nucleoside conformers that are CT quenched much more slowly than the majority of conformers. Thus the emission spectra in Figure 6 arise from PAdU conformers with slow CT quenching rates.

For PAdU a two dimensional matrix of emission lifetime with solvent rows and wavelength columns shows a pattern of a decreasing number of wavelengths from blue to red having multicomponent emission lifetimes and a correspondingly increasing number of wavelengths from red to blue having only a single emission lifetime (≤0.1 ns) as solvent is changed from THF to MeCN and then to MeOH.[29] Thus as CT quenching increases for PAdU in this solvent series, the number of wavelengths with ultrashort emission lifetimes increases from only one at 600 nm in THF, to two at 550 and 600 nm in MeCN, and finally to three at 500, 550, and 600 nm in MeOH. In THF emission from PAdU has a single second lifetime component that monotonically decreases from 8.0 to 6.3 ns over the 386–550 nm range. In MeCN and MeOH pyrenyl emission from PAdU has both

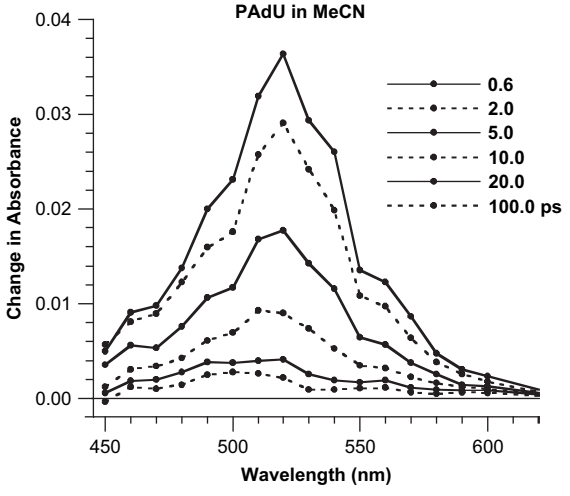

Figure 7. Overlayed TA spectra for PAdU in MeCN at the indicated times after photoexcitation with 100 fs duration (fwhm) pulses at 400 nm. Adapted with permission from the Journal of Physical Chemistry A.[30] Copyright 2005 American Chemical Society.

second and third lifetime components. In MeCN these lifetimes are 4.6 ns (0.24 amplitude) and 12 ns (0.09) at 415 and 440 nm, but most of the pyrenyl emission at these two wavelengths decays in 0.7±0.4 ns (0.67). At the same time, the majority of all TA (from both pyrenyl $^1(\pi,\pi^*)$ and CT states) lives only 5 ps. In MeOH most of the emission decays in ≤0.1 ns (0.92–0.98) over the full spectral range 384–600 nm; over the 384–440 nm pyrenyl emission range the second and third lifetime components are 4 ns (0.05–0.01) and 23–7 ns (0.03–0.01). Consistent with increased CT quenching, the amplitude of the subnanosecond lifetime component increases from 0.67 to 0.98 over most of the pyrenyl wavelength range on going from MeCN to MeOH. Similarly the triple-component PAdU emission kinetics pattern with second and third lifetime components that decrease in amplitude and wavelength range from blue to red in the THF, MeCN, and MeOH solvent series is also consistent with increasing CT product stabilization in this solvent series. Finally the nucleoside/solvent combination (i.e., PAdU/MeOH) with the lowest emission quantum yield in Table 3 also has the shortest average pyrenyl emission lifetimes and a CT state that lives only for 6 ps.

2.1.7. $P^{\bullet+}/dU^{\bullet-}$ CT state stabilization by MeOH. The exceptional stabilizing influence of MeOH compared to MeCN on CT product formation can be seen in Table 3 by noting that ϕ_{em} generally decreases (due to increasing CT quenching) in MeOH compared to MeCN i.e., for PdU 0.35→0.027, for PCOdU 0.005→0.002, and for PAdU $0.97\times10^{-3}\rightarrow0.08\times10^{-3}$.[20,21] (For PMAdU this effect can be seen by noting that the amplitude of the subnanosecond component of pyrenyl emission at 395 nm increases from 0.22 to 0.81 on going from MeCN to MeOH.[31]) Although MeOH and MeCN have similar dielectric constants (ε) 33.6 and 37.5, respectively, MeOH enhances CT quenching of pyrenyl emission much more than does MeCN for these four nucleoside conjugates. Clearly the hydrogen bond donating ability of MeOH is likely the reason. Netzel had earlier proposed that a the uracil anion in the CT state was protonated in MeOH forming $P^{\bullet+}/dU(H)^{\bullet}$.[21] However, Wagenknecht and co-workers correctly pointed out that the pK_a of $dT(H)^{\bullet}$ as measured by Steenken[32] (and presumably also the pK_a of $dU(H)^{\bullet}$) was 6.9, while the pK_a of MeOH was 15.7.[33] Thus based on acidities, $MeOH+dU^{\bullet-}$ products are thermodynamically favored over $MeO^-+dU(H)^{\bullet}$ products. Exceptional CT product stabilization (as evidenced by greatly increased pyrenyl emission quenching) in MeOH compared to equally polar MeCN should therefore be ascribed to hydrogen bond formation by MeOH with the $P^{\bullet+}/dU^{\bullet-}$ CT product, perhaps denoted as $MeOH\cdots dU^{\bullet-}/P^{\bullet+}$.[33]

2.1.8. CT state energies in PdU, PCOdU, PMAdU, and PAdU. It is instructive to examine the ϕ_{em} values for THF in Table 3 for the compound series PdU, PCOdU, PMAdU, and PAdU, respectively, 0.420, 0.028, 0.016, and 0.0018. Similar decreasing ϕ_{em} series are also found for these nucleosides in MeCN and MeOH. As noted earlier, attaching CO to C5 uracil in PCOdU is expected to maker uracil easier to reduce and thus to lower the energy of a $P^{\bullet+}/dU^{\bullet-}$ CT excited state relative to that in PdU; this is consistent with a lower ϕ_{em} for PCOdU compared to PdU in THF. In PAdU the CO attachment to uracil in PCOdU remains, but an amino

group is attached to pyrene to form an amido linker. Amino substituted pyrene is easier to oxidize than pyrene so PAdU should have a lower energy CT state than either PCOdU or PdU. This expectation is born out by noting that PAdU has the lowest ϕ_{em} for the nucleoside series in each of the three solvents in Table 3. PMAdU tests the above reasoning further by inserting a methylenyl group between pyrene and the amido linker. PMAdU retains the CO attachment to uracil found in PCOdU but no longer has the ease of oxidation of an aminopyrene. Thus PMAdU should have a CT state energy similar to that of PCOdU. Indeed ϕ_{em} values for PMAdU are reasonably similar to those for PCOdU in the corresponding solvent given that the pyrenyl group is more flexibly tethered with three linking atoms in PMAdU and more rigidly fixtured with a single linking atom in PCOdU.

2.1.9. PMAdU. Above 310 nm where uracil does not absorb, the absorption and emission spectra for PMAdU look identical to those for the PAAc, a spectroscopic model of a pyrenyl chromophore whose $^1(\pi,\pi^*)$ state cannot be CT quenched. Emission from PAAc decays with a single exponential lifetime of ca. 250 ns in THF, MeCN, and MeOH. As expected pyrenyl emission in PMAdU is quenched relative to that from PAAc in the corresponding solvents, respectively, 75%, 98%, and 90%. Given that the energy of the $P^{\bullet+}/dU^{\bullet-}$ CT state is similar in PMAdU and PCOdU it is interesting to see what effect the flexible, three atom linker has on the lifetime of the CT state compared to the 69 ps lifetime found for PCOdU in MeOH. Table 4 reports that PMAdU emission at 550 nm in MeOH has three lifetime components and that the normalized average lifetime based on the two major components (0.96 total amplitude) is 2.1 ns. Not unexpectedly for the PMAdU nucleoside with a three atom linker, multiexponential emission decays are seen at all wavelengths in all three of the above solvents.[31] In THF four decay lifetimes are present at all wavelengths from 375 to 550 nm and spanning lifetimes from 0.5 to 290 ns. The longest component, however, has only 0.01 amplitude. In the two polar solvents no more than three decay lifetimes are present and the amplitudes of rapidly quenched (<10 ns) pyrenyl emission at 395 nm are larger than in nonpolar THF, respectively, in MeCN and MeOH 0.92 and 0.88 versus 0.31 in THF. The increase in fast pyrenyl $^1(\pi,\pi^*)$ quenching on going from THF to the polar solvents is consistent with expected CT state stabilization in the latter solvents.

Table 4. Pyrenyl–dU CT state lifetimes in MeOH

Nucleoside	CT lifetimes, ns (amplitude)	Average CT lifetime, ps
PdU	0.12 (0.47) 0.91 (0.53)[a]	540[b]
PCOdU	0.069[c]	69
PMAdU	0.80 (0.57) 4.1 (0.39) 66 (0.04)[d]	2,100[e]
PAdU	0.006[f]	6

[a] Emission lifetime at 560 nm.[20] This nucleoside was also measured by TA in buffer at pH 8 and found to have 'a lifetime in the range of several nanoseconds'.[99] A second report of the TA study of PdU in buffer at pH>7 states, 'we could show that the lifetime of the charge-separated species $Py^{\bullet+}$–$dU^{\bullet-}$ is in the range of a few nanoseconds…'.[100]
[b] Average emission lifetime equals the sum over all lifetimes of amplitude times lifetime.
[c] Picosecond TA measurement (see Fig. 5).[21]
[d] Emission lifetime at 550 nm.[31]
[e] Average emission lifetime equals the normalized sum of amplitude times lifetime over the two major lifetime components.
[f] Femtosecond TA measurement.[30]

A number of factors in addition to the free energy of reaction affect electron transfer rates. For nonadiabatic CT these include inner and outer sphere reorganization energies and electronic coupling.[34–38] Given the common nature of the CT reaction and similarly fixtured donor and acceptor subunits in PdU, PCOdU, and PAdU, it is reasonable to assume that the reorganization energy and electronic coupling are similar within this three member series. If so, changes in the energy of the $P^{\bullet+}/dU^{\bullet-}$ CT excited state are likely to be dominant contributors to CT rate differences among these nucleosides. Note that the pyrenyl $^1(\pi,\pi^*)$ electronic origins are similarly located for both absorption and emission within this nucleoside series. With these thoughts in mind, it is easy to explain the CT state lifetime shortening from ca. 540 ps to 6 ps as one proceeds from PdU to PAdU as being due to a decreasing energy gap for charge recombination in the Marcus inverted region.[36,39–43] In this CT region, the absolute free energy of charge recombination exceeds the sum of the reorganization energies, and decreases in the absolute free energy of reaction result in increased charge recombination rates (i.e., decreased CT state lifetimes).

Against this background the 2.1 ns average lifetime for the major CT emission lifetime components of PMAdU at 550 nm in MeOH can be seen as striking. Note that pyrenyl $^1(\pi,\pi^*)$ emission does not extend beyond 465 nm in these nucleoside conjugates. Thus the red emission beyond 500 nm provides a direct measure of the lifetime of their CT states. Indeed many PMAdU conformers (0.39 emission decay amplitude) live for 4.1 ns, and a much smaller fraction (0.04 emission decay amplitude) lives for a remarkable 66 ns. If PMAdU had the same reorganization energy and electronic coupling as PCOdU the average lifetime of its CT state would be expected to be ca. 70 ps. The much longer average CT state lifetime in many PMAdU conformers compared to PCOdU is likely due to a combination of lessened electronic coupling, increased CT state energy (in extended conformations of the three atom linker compared to a one atom carbonyl linker), and reduced inner sphere reorganization energy (resulting from greater isolation of pyrenyl cation distortions from the linking atoms in PMAdU compared to PAdU). The important result is that appropriate fixturing of the pyrenyl and dU subunits in pyrenyl–dU conjugates can produce $P^{\bullet+}/dU^{\bullet-}$ CT excited states (or photoproducts) with lifetimes of several nanoseconds. The challenge for those who would wish to use $P^{\bullet+}/dU^{\bullet-}$ CT states in molecular electronics, medical diagnostics, or sensing applications is to develop ways of accomplishing the required fixturing.

2.2. Electronic structure calculations for pyrenyl–dU nucleoside conjugates

2.2.1. In vacuum calculations for PAdU. Before discussing electronic structure calculations for either PAdU or PMAdU, it will be helpful to point out that their structures drawn in Figure 3 have *trans*-amido bonds (i.e., the carbonyl and NH groups are trans with respect to the C–N amido bond). Analogies with the structures of related *N*-monosubstitued

amides and the NMR spectrum of PAAc imply that PAAc, PAdU, and PMAdU have *trans*-amido bonds. Additionally, PM3 semiempirical computations on *N*-(1-pyrenyl)-1-methyluracil-5-carboxamide (PAU_{Me}, a model of PAdU with a methyl group in place of the sugar) also found trans-isomers to be lower in energy than cis-isomers.[29] For these reasons the following discussion will concentrate on computational results for *trans*-amido conjugates and only occasionally review findings for *cis*-amido ones.

Both TA and emission kinetics results on the pyrenyl–dU nucleosides discussed above indicated that these compounds exist in solution in a variety conformations. Several electronic structure studies have been carried out for models of the above nucleosides to learn what factors might be controlling the energies of their CT states and how large might be the energy variation of these states within an ensemble of conformers. The first studies addressed these questions in vacuum,[29,31] but follow-on studies incorporated solvent effects based on dielectric continuum[44] (or Onsager theory)[45] and Discrete Reaction Field[46] (DRF) solvent models. The first such study examined PAU_{Me} with PM3 computations to establish an ensemble of eight trans-conformers in their ground states. Next INDOs/CIS (Intermediate Neglect of Diatomic Overlap/Configuration Interaction Singles) vertical, excited state computations were carried on each conformer. Not surprisingly for an in vacuum study, all conformers had pyrenyl (π,π^*), lowest energy singlet excited states (P_1); their energies spanned only a narrow range 3.74–3.76 eV. In contrast, the lowest energy singlet $P^{\bullet+}/dU^{\bullet-}$ CT states (CT_1) spanned 3.80–4.32 eV! As follow-on studies showed, polar solvents lowered the energy of the CT_1 states below the energy of the P_1 states. However, in vacuum studies provide a basis for understanding solution results and show core electronic effects in the absence of complications that may arise from approximate solvent models.

Transitions were identified by the types of orbitals involved. For example CT transitions involved excitation of an electron in a pyrenyl occupied molecular orbital (OMO) to a uracil unoccupied molecular orbital (UMO). Additionally, CT states had dipole moments larger than 10 D (generally in the range 14–30 D), while pyrenyl (π,π^*) excited states (P_n) had dipole moments less than 10 D (generally 2–8 D). One major finding was that the energy of the uracil LUMO (lowest UMO) was linearly correlated with the absolute value of the dihedral angle between the linking carbonyl and the C5–C4 uracil bond (CO/U_{Me} dihedral angle). When the CO group is nearly in the plane of the C5–C4 bond (i.e., the absolute value of the dihedral angle is small), the energy of the uracil LUMO is low and U_{Me} is easy to reduce. The opposite is true when the CO group is out of the plane of the C5–C4 bond. For *trans*-PAU_{Me} isomers there is also a linear correlation of energy of the CT_1 state with the energy of the uracil LUMO. Thus the CO/U_{Me} dihedral angle is a major, but not the only factor that controls the variation of the CT_1 state's energy.

The other factor influencing the CT_1 state's energy is Coulombic stabilization of the cationic and anionic subunits with decreasing distance of separation. Thus two PAU_{Me} conformers with the same CO/U_{Me} dihedral angle would have different CT_1 energies if their pyrenyl and uracil subunits were differently spaced: the conformer with closer subunits would have a lower CT_1 energy. Detailed studies of CT_1 energies at various subunit separations showed that the stabilization interaction varied as $1/R$, where R was measured from the center of the pyrenyl ring to the center of the uracil ring. A linear plot of the dipole moment of the CT_1 state versus R yielded a slope equal to the charge of one electron. Finally, the extrapolated CT_1 energy at $R=\infty$ was equal to the energy of the pyrenyl HOMO to uracil LUMO gap, as expected for infinitely separated $P^{\bullet+}$ and $dU^{\bullet-}$ products within the Hartree–Fock (HF) approximation (i.e., Koopmans theorem).[47,48]

The third important observation from the INDOs/CIS vacuum study of PAU_{Me} was that variation of the CO/U_{Me} dihedral angle controlled not only the energy of the uracil LUMO but also the extent of this LUMO's delocalization onto the linking amido atoms. The consequence of this on the dipole moments of the CT_1 state was dramatic. For example, two conformers with similar subunit separations could have a CT_1 dipole moment difference of 12 D due to having different CO/U_{Me} dihedral angles: the conformer with the lower absolute value of the CO/U_{Me} dihedral angle would have both a lower CT_1 energy and a smaller dipole moment due to more LUMO delocalization onto the linking atoms. We will see below that in solution the size of a CT state's dipole moment is very important.

2.2.2. In vacuum calculations for PMAdU. To test the generality of the above conclusions based on electronic structure calculations for PAU_{Me}, a similar study was carried out for $PMAU_{Me}$ (*N*-(1-pyrenylmethyl)-1-methyluracil-5-carboxamide, a model of PMAdU with the sugar replaced by a methyl group).[31] Random conformational searching by varying the angles of the four linking bonds yielded 11 trans-conformers and 8 cis-ones. Here we will concentrate on the results for the experimentally relevant trans-conformers, except to note that the heat of formation energies for all trans-conformers were less than those for the cis-conformers. At room temperature these energies for the 11 trans-conformers spanned the energy range $(0.0–3.6)\times k_BT$, where k_B is the Boltzmann constant. The energies of the pyrenyl P_1 states of for all 19 conformers were independent of conformer geometry. For the trans-conformers, the dipole moments of the P_1 states ranged from 2.5 to 3.9 D, while those of the CT_1 states ranged from 11 to 31 D. Finally, for CT_1 states the HOMO was a pyrenyl orbital and the LUMO was a uracil orbital.

An excellent linear correlation ($R=0.90$) was found for all 19 $PMAU_{Me}$ conformers for the energy of the uracil LUMO versus the absolute value of the CO/U_{Me} dihedral angle (here defined as the angle between the linking carbonyl and the C5–C6 alkenyl bond in uracil). The linear correlation between the energy of the CT_1 state and the energy of the uracil LUMO was strong ($R=0.78$) but not excellent. The spread of CT_1 energies at several CO/U_{Me} dihedral angles indicated that Coulombic stabilization in addition to the energy of the LUMO was important in determining the energy of the CT_1 state. A quantitative definition of the magnitude of CT_1 Coulombic stabilization (defined to be positive) is the energy difference between the HF (Hartree–Fock) HOMO–LUMO energy gap and the CT_1 state's

energy. Typically this stabilization energy is in the order of 2 eV for a *trans*-$PMAU_{Me}$ conformer. As in the study of PAU_{Me}, $PMAU_{Me}$ conformers with similar CO/U_{Me} dihedral angles had different CT_1 state energies if they had different subunit separation distances, with smaller separations yielding lower CT_1 state energies.

Interestingly the uracil LUMO extended to various degrees onto the amido linkage for all trans-conformers. This had the consequence that the dipole moments of the CT_1 states depended on both the distance of separation of the pyrenyl and uracil subunits and on the distribution of the uracil LUMO. For example, one trans-conformer had a smaller subunit separation distance than another yet also had a CT_1 state dipole moment of 19 compared to 11 D in the latter conformer. Both had comparable delocalization of their uracil LUMOs onto their respective amido linkers, thus this LUMO distribution effect on CT_1 state dipole moment is not the same as the LUMO delocalization effect discussed above for PAU_{Me}. Rather in the first conformer with the smaller subunit separation, the uracil LUMO extended strongly to the far side of the uracil away from the linker. In the second conformer with the larger subunit separation, the uracil LUMO was concentrated on the C4–C5–C6 uracil carbons near the amido linker. The consequences were that the anionic charge of the CT_1 state in the first case was shifted farther away from the cationic charge of the pyrenyl subunit than in the second case. Together the INDOs/CIS studies of PAU_{Me} and $PMAU_{Me}$ show that the size of the dipole moment of CT_1 states depends both on the degree of uracil LUMO delocalization onto the linking atoms and on the distribution of the uracil LUMO itself. Lastly, the earlier conclusions from the PAU_{Me} study concerning the affect of the CO/U_{Me} dihedral angle on the energies of the uracil LUMO and the CT_1 state and the affect of subunit separation on the Coulombic stabilization of the CT_1 state were confirmed in the $PMAU_{Me}$ study.

2.2.3. Dielectric continuum calculations for PAdU. As noted above for the INDOs/CIS studies of PAU_{Me} and $PMAU_{Me}$ in vacuum, all CT_1 state energies were higher than the pyrenyl $^1(\pi,\pi^*)$ P_1 state energies. Thus in vacuum $P^{\bullet+}/dU^{\bullet-}$ CT quenching of P_1 states was predicted to be endergonic. Clearly solvation effects must be modeled to account for the experimental observations of CT quenching in polar solvents. There are a number of ways of modeling solvent in electronic structure computations. The simplest is to model the solvent as a dielectric continuum with the solute located in a spherical cavity of radius a_0. This is the Onsager model[45] and uses the solute's dipole to polarize the dielectric continuum and create a self-consistent reaction field (SCRF). Then the solvent SCRF interacts with the solute to produce SCRF HF self-consistent field (SCF) ground state orbitals. The major drawback to this model is that the cavity radius is at best a phenomenological parameter (i.e., it is not a physical entity). Arguslab 1.0 (β build #2)[47,49,50] computed the SCRF HF SCF ground state orbitals for PAU_{Me} for specified solvent cavities and then carried out a CIS excited state computation using these ground state orbitals.[44] The ArgusLab implementation of SCRF INDOs/CIS was the same as method A in the 1992 paper by Karelson and Zerner.[51] Importantly, Arguslab applied post-CI first-order correction for polarization to the excited state energies. It neglected second-order corrections for differential solvation of ground and excited states. In this dielectric continuum work on PAU_{Me} as in the previous in vacuum studies, vertical excitation energies (as observed in electronic absorption) were calculated. For the CIS computations 10 HOMO and 10 LUMO orbitals were included as increasing the number of these orbitals did not affect the energies of the lowest several, excited singlet states. Questions concerning the energy of relaxed CT states, therefore, were not addressed in this work. Such relaxed CT states are important for a complete assessment of whether or not P_1 states will be CT quenched in solution and these affects will be discussed below with the aid of a more accurate solvent model.

In the dielectric continuum study of PAU_{Me} the solvent cavity radius was varied for each of the eight trans-conformers investigated to give as good as possible spectral agreement with the absorption spectrum of PAdU in MeCN without changing the energy of the conformer's P_1 state. Radius values were typically 4.1–5.0 Å; the continuum's dielectric constant (ε) and refractive index (η) were set to 40 and 1.3, respectively, close to the values for MeCN. In the vacuum studies above, there was no correlation between the energy of a CT_1 state and its dipole moment. In contrast in solution there was a strong correlation between these quantities (R=0.90 for trans-conformers). Additionally the ranking of conformers in terms of the energy of the CT_1 state was very different in vacuum and in solution. Understanding these changes in CT_1 state energy upon going from vacuum to solution requires examining how solvation affects the Coulombic stabilization of $P^{\bullet+}/dU^{\bullet-}$ CT states. One affect is that the strength of Coulombic stabilization is reduced due to solvent screening of the charges on the ionic subunits. Thus for CT states with small dipole moments (generally $\leq$20 D), dielectric screening raises the energy of CT states upon solvation. However, for CT states with large dipole moments, direct solvent reaction field stabilization of the excited state's dipole dominates the Coulombic screening energy loss and produces a lowering of the CT state's energy upon solvation. For example, three conformers with CT_1 solution phase dipole moments of 26, 24, and 29 D had solvation energy decreases, respectively, of 0.58, 0.66, and 0.96 eV. In contrast for another conformer whose CT_1 state had a solution phase dipole moment of 20 D, the CT_1 state's energy increased from 3.55 to 3.90 eV upon solvation.

One interest in computational studies of pyrenyl–dU nucleoside conformers is to learn the range of CT_1 state energies that might occur. In vacuum for PAU_{Me}, CT_1 state energies for trans-conformers spanned a range of 0.5 eV. For the same eight trans-conformers with solvation modeled as dielectric continuum the range of CT_1 state energies was 1.0 eV (3.07–4.08 eV). This range of CT_1 energies is surprisingly large and is consistent with a wide range of CT quenching lifetimes for pyrenyl $^1(\pi,\pi^*)$ emission.

The CIS method of computing excited state energies builds upon the ground state HF molecular orbitals. However, the energies of these UMOs reflect their energy when all of the OMOs are full. Excited states in contrast have one less electron in the HF OMOs and one more electron in the HF UMOs than the ground state. In excited states, the singly occupied HF UMOs relax in energy because of Coulombic

attraction between them and the one-electron deficient set of HF OMOs in the presence of the full nuclear charge. The CIS method accomplishes this relaxation of the partially occupied HF UMOs by constructing single excitation determinants and solving for their coefficients. The excited states produced by the CIS method are thus characterized by coefficients corresponding to the weighting of the particular single excitation determinants that comprise each state. It is, therefore, natural to analyze CIS excited states according to the major determinant coefficients of each state. For convenience, these single excitation determinants are referred to as orbital transitions here.

In fact the P_1 state of *trans*-PAU_{Me} conformers that have good agreement between their computed absorption spectra and the observed absorption spectrum for PAdU in MeCN arises from as many as five orbital transitions. In a typical conformer, three of these are dominant, and all three originate in pyrenyl OMOs. Not unexpectedly key properties of the P_1 state of PAU_{Me} are almost the same as those for the same state in PAAc: energy (3.47 vs 3.43 eV, former vs latter), oscillator strength (0.007 vs 0.012), and dipole moment (5.2 vs 6.1 D). Yet of the three dominant orbital transitions that comprise P_1 in PAU_{Me}, the largest and the third largest terminate in uracil UMOs. In fact six of the eight *trans*-PAU_{Me} conformers studied have P_1 states with a dominant (largest absolute value CI determinant coefficient) pyrenyl OMO to uracil UMO orbital transition. Clearly the P_1 state of PAAc does not have this CT contribution. Indeed the emission spectrum of PAdU in MeCN in Figure 6 is red-shifted and much broader than the pure $^1(\pi,\pi^*)$ emission spectrum of PAAc in THF, MeCN, and MeOH.[29] As discussed above the emission from PAdU in MeCN arises from a minority of conformers that are slow to CT. The dielectric continuum INDOs/CIS calculations for most *trans*-PAU_{Me} conformers suggest that the emitting PAdU conformers in MeCN likely have mixed P_1 and $P^{\bullet+}/dU^{\bullet-}$ CT character. Such a mixed P_1/CT character for the emitting states of PAdU in MeCN (and by analogy also in MeOH) would be consistent with their observed broad, red-shifted emission spectrum.

As discussed above for PAU_{Me} and $PMAU_{Me}$ in vacuum, the absolute value of the CO/U_{Me} dihedral angle controls both the energy of the uracil LUMO (and therefore the ease of reduction of uracil) as well as the delocalization of this orbital onto the linking atoms. In vacuum, such orbital delocalization does not influence the energy of the CT_1 state whereas the energy of the uracil LUMO does. In a solvent according to the dielectric continuum model, however, the dipole moment of a CT state is a very important determinant of that state's energy due to the dipole's interaction with the solvent reaction field. Thus an ironic inversion of CT energies occurs on going from vacuum to solution. In vacuum conformers with large absolute value CO/U_{Me} dihedral angles have high CT_1 state energies, little uracil LUMO delocalization, and large dipole moments. In a polar solvent, these same conformers have low CT_1 state energies precisely because they have little uracil LUMO delocalization, and large dipole moments. In contrast, conformers with small absolute value CO/U_{Me} dihedral angles in vacuum have low CT_1 state energies, significant uracil LUMO delocalization and small dipole moments. In a polar solvent, these conformers have high CT_1 state energies precisely because they have significant uracil LUMO delocalization and small dipole moments. Thus for conformers with large absolute value CO/U_{Me} dihedral angles, the disadvantage (with respect to forming a low energy CT_1 state) of having a hard to reduce uracil subunit is completely reversed in a polar solvent by the advantage of having a localized uracil LUMO.

2.2.4. Discrete reaction field (DRF) calculations for PAdU. Although it was a significant improvement over vacuum studies, the just discussed SCRF INDOs/CIS electronic structure study of PAU_{Me} in solution with the solvent modeled as a dielectric continuum suffered several drawbacks. The first was that the solvent cavity in the continuum model was non-physical. Others were that neither the solute's nor the solvent's geometry was relaxed for the CT states. This meant that the energies of solvent equilibrated CT_1 states following CT from pyrenyl $^1(\pi,\pi^*)$ states were not calculated; rather only vertical excitation energies were examined. In the work to be discussed next, INDOs/CIS was combined with explicit solvent molecules in place of the dielectric continuum, and the solvent was relaxed about the charge distribution of the CT_1 vacuum states. Thus both vertical and solvent relaxed CT_1 state energies were computed for PAU_{Me} in MeCN.[46] In this work a discrete reaction field (DRF) solvation model was used in which MeCN was represented by discrete molecules that were characterized by atomic charges, polarizabilities, and radii. Molecular dynamics (MD) techniques were used to equilibrate solvent around the charge distribution of the solute (or, rather a classical representation of that distribution) in any specified electronic state. The advantages were many: no unphysical parameters, ample attention to microscopic detail, and inclusion of specific solute/solvent interactions like hydrogen bonding. The only disadvantage was that the discrete solvent model was computationally more demanding than the dielectric continuum model; true for the greater part because of the need for MD simulations.

Figure 8 summarizes the kinetics events following photoexcitation of a solution of PAdU nucleoside in MeCN and emphasizes the fact that PAdU exists as an ensemble of different conformers each with a variety of solvent configurations. The energy of the $P^{\bullet+}/dU^{\bullet-}$ CT states of most conformers in most solvent environments is too high to permit CT immediately following light absorption.[29,44] This is true because the solvent configuration immediately following vertical photoexcitation is the same as that of the nucleoside's ground state (Frank Condon principle). For very polar excited states (such as most $P^{\bullet+}/dU^{\bullet-}$ CT states) in polar solvents, solvent orientation has a large effect on excited state energy. Note that emission from CT_1 states with CT-equilibrated solvent (red levels) terminates in S_0 states also with CT-equilibrated solvent (red levels). These latter S_0 states are higher in energy than the corresponding S_0 states with GS-equilibrated solvent. Figure 8 ignores energy differences between P_1 and S_0 states with P_1-equilibrated solvent (the states responsible for pyrenyl emission) and the same states with GS-equilibrated solvent (the states responsible for pyrenyl absorption). However, the small Stokes shift between the absorption and emission origins for PAAc in MeCN justifies this neglect. Thus the increased energy of S_0 states and the decreased energy of CT_1 states both with

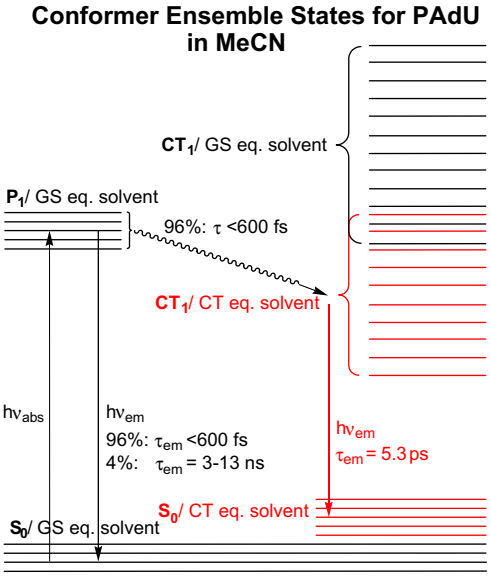

Figure 8. An electronic energy level diagram for an ensemble of PAdU conformers in MeCN. S_0 is the ground state (GS); P_1 is the lowest energy pyrenyl $^1(\pi,\pi^*)$ state; and CT_1 is the lowest energy $Py^{\bullet+}/dU^{\bullet-}$ charge transfer state. The indicated emission and CT_1 formation lifetimes (τ) are discussed in the text. Importantly, the multiple levels for each state represent multiple electronic origins arising from different PAdU conformers each with numerous solvent configurations. The dispersion of electronic origins is much larger for the CT_1 states than for the P_1 states; for the former it depends strongly on whether the solvent surrounding the CT_1 state is equilibrated with the charge distribution of the ground (GS eq. solvent) or CT_1 (CT eq. solvent) state. Adapted with permission from the Journal of Physical Chemistry A.[46] Copyright 2006 American Chemical Society.

CT-equilibrated solvent (i.e., compared to the corresponding states with GS-equilibrated solvent) are responsible for the much lower energy of the $P^{\bullet+}/dU^{\bullet-}$ CT emission seen in MeCN for the PAdU nucleoside compared to the pyrenyl emission seen for the PAAc spectroscopic model in the same solvent.

2.2.5. The discrete reaction field approach. In the DRF[52–55] approach a solute is described by some quantum mechanical method (the QM system), while the solvent is modeled via molecular mechanics by any number of discrete molecules and—optionally—an enveloping dielectric continuum (the MM system). The permanent charge distribution of a solvent molecule is represented by point charges, mainly at the constituent atoms, but more sites may be used to represent multipole moments beyond the dipole moment. The needed charges are obtained from appropriate quantum chemical calculations.[56,57] Changes in the solvent's charge distribution, due to interactions with other parts of the system, are taken care of by putting polarizabilities located either at the atoms (distributed polarizability model) or at appropriate centers (group polarizability model). Polarizabilities are obtained by appropriate quantum chemical calculations or by fitting to experimental results.[58–60]

The DRF was implemented for single determinant (RHF, ROHF, and UHF) wave functions with the standard INDO parameterization (DRF INDO).[47,61] For calculating spectra INDOs/CIS was used. Since INDO is intrinsically a minimal basis set approach, expanded electric fields and reaction potentials were used for evaluating the solute/solvent interactions with the solute's nuclei and center of mass as expansion centers; thus all needed integrals were obtained as linear combinations of overlap and dipole integrals.[54] By default, no two-electron DRF integrals were computed for the SCF ground state, since the average reaction field formulation was used. Thus the dispersion interactions were not calculated.

2.2.6. DRF computational procedures. Eight PAAc conformers were obtained for study by rotating the *N*-acyl group in steps of 45° from the fully planar structure. The latter was replaced by the gas phase optimized structure. For PAU_{Me} eight conformers each at a local energy minimum were taken from a previous SCRF INDOs/CIS study.[44] Each of the conformers were subject to a DFT calculation using the Amsterdam Density Functional[62] (ADF) package for generating the heats of formation. The resulting heats of formation showed that all of the conformers for both compounds were thermally accessible. In the MD simulations the solutes' charge distributions were represented by atomic effective charges from the corresponding vacuum INDO calculations. INDO atomic charges reproduce the dipole moments of electronic states fairly well. Although ADF calculations generate better point charges[57] for the ground state, they do not describe excited states very well. Thus, for consistency INDO charges were used throughout this work.

Separate classical MD simulations were performed for each conformer immersed in 100 MeCN molecules using the DRF90 program[63] with rigid solute and solvent molecules and a time step of 1 fs at a temperature of 298 K controlled by a Nosé–Hoover thermostat[64] in an NVT ensemble. The molecules were placed in a virtual sphere with a radius of about 28 Bohr, and a soft wall-force[65] was applied to keep the molecules from evaporating. Equilibration runs of about 20 ps were performed, followed by 50-ps production runs from which 100 uncorrelated solute/solvent configurations were selected and saved. This was sufficient to retain all statistically significant solute/solvent information.[66] In fact two series of such MD simulations were run for each conformer, one for the solvent equilibrated with respect to the conformers' ground state charge distribution and the other for the solvent equilibrated with respect to the first vacuum $P^{\bullet+}/dU^{\bullet-}$ CT excited state for PAU_{Me} conformers and to the first vacuum $^1(\pi,\pi^*)$ excited state for PAAc conformers.

From the first MD series, DRF INDOs/CIS was used to calculate the energies of the 20 lowest energy electronic states, their dipole moments, and the oscillator strengths connecting them with the ground state. Each conformer's oscillator strengths were scaled with Boltzmann factors obtained by combining the ADF vacuum energies and the classical MD energies for each solvated conformer, and 800 solute/solvent configurations were combined to form a single ensemble. Ensemble absorption spectra for each compound were generated by adding the Boltzmann weighted oscillator strengths for each family of conformers in 200 intervals of equal energy-width over a wavelength region from about 200 nm to 370 nm. Emission spectra were calculated similarly, but without Boltzmann weighting, from the second MD series using only either the lowest energy excited state or the two lowest energy excited states. In summary, for each compound and for both absorption and emission

spectra, 800 statistically significant solute/solvent configurations (based on eight different solute conformers) were obtained and used to calculate 20 electronic excited states. Consequently, each simulated band spectrum was based on 15,200 computed transitions.

2.2.7. DRF INDOs/CIS absorption spectra for PAAc and PAU_{Me}. Figure 9 presents calculated absorption and density of excited states (DOS) spectra for PAAc (top) and PAU_{Me} (bottom) in MeCN. For PAAc the calculated spectra show very weak absorption in the forbidden S_1 region, broad absorption in the S_2 region, and sharp, very strong absorptions around 257 and 236 nm. The first of these appears to be two closely spaced electronic transitions at 258 and 256 nm. Indeed the second strong absorption band observed experimentally also appears to consist of two closely spaced transitions at 282 and 276 nm. Overall the pattern of three regions of strong absorption and one of forbidden absorption found experimentally for PAAc is well reproduced in the calculated absorption spectrum. The greatest failing of the DRF INDOs/CIS absorption spectrum of PAAc is that its bands are on average 0.24 (σ ±0.12) eV blue-shifted with respect to the experimental bands. This failing appears to be due to the earlier noted neglect of dispersion in these calculations. The top panel in Figure 9 also shows a plot of calculated DOS versus wavelength for PAAc. These results show that the electronic manifold of PAAc is much richer than the absorption spectrum alone suggests. In particular, high numbers of forbidden excitations are seen in four regions: 360, 295, 225, and 205 nm.

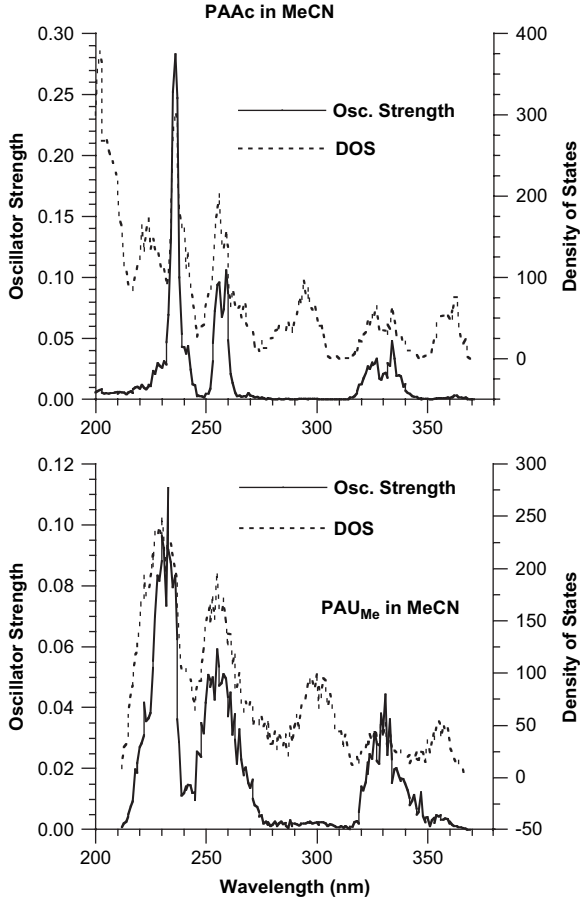

Figure 9. Plots of DRF INDOs/CIS calculated oscillator strength (absorption) versus wavelength and density of excited states (DOS) versus wavelength spectra for PAAc (top) and PAU_{Me} (bottom). Both types of spectra are Boltzmann weighted statistical averages of the individual spectra for eight PAAc or PAU_{Me} conformers each with 100 MeCN configurations. Appropriate Boltzmann factors were calculated based on the relative energy of each solute/solvent configuration. In turn, these relative configuration energies were determined by summing the vacuum ADF energy of the corresponding PAAc or PAU_{Me} conformer with its classical solute configuration energy equilibrated via MD about the charge distribution of the solute's ground state. Spectra were calculated by summing the occurrences of Boltzmann weighted oscillator strength for excited states in each of 200 equal-width energy intervals over the plotted wavelength range. Adapted with permission from the Journal of Physical Chemistry A.[46] Copyright 2006 American Chemical Society.

The bottom panel of Figure 9 shows the calculated absorption spectrum for PAU_{Me} in MeCN. Two features are striking. One, the calculated absorption bands are much broader for PAU_{Me} than for PAAc. This agrees with the experimental absorption spectra for PAdU and PAAc in MeCN. Two, the absorption bands for PAU_{Me} at 255 and 232 nm are, respectively, about 1.5- and 2.9-fold less intense than the corresponding sharp absorption bands of PAAc. Apparently, the allowed oscillator strength in the sharp bands of PAAc is redistributed among a larger number of states in PAU_{Me}. A similar, but less large relative absorption drop is seen experimentally in MeCN where the ratio of the 242- to 340-nm bands of PAAc is 1.93, but decreases in PAdU to 1.35 for the ratio of the 238- to 358-nm bands. As a result of oscillator strength redistributions on going from PAAc to either PAU_{Me} or PAdU, both pyrenyl-uracil conjugates have absorption spectra with three main bands that are not too different in intensity and that monotonically decrease on going from short to long wavelengths.

The positions of the three main absorption bands for PAU_{Me} and PAAc in Figure 9 are much the same. This is expected since they would have to shift due to differences in dispersion, and this interaction is neglected here. Similarly the general locations of the bands of PAAc and PAdU do not differ very much. Most of their apparent band shifting is due to two effects: wider absorption bands and much more red-edge absorption in the S_1/S_2-region for PAdU compared to PAAc. The bottom panel in Figure 9 shows a plot of calculated DOS and oscillator strength spectra for PAU_{Me}. By comparing these two spectra, high numbers of forbidden excitations can be seen in the 360- and 300-nm regions. This is very similar to the DOS and oscillator strength patterns seen in the top panel of Figure 9 for PAAc. For both molecules allowed absorption intensity arises from $\pi \rightarrow \pi^*$ transitions. In PAU_{Me}, $P^{\bullet+}/dU^{\bullet-}$ CT states borrow oscillator strength if they are near allowed (π,π^*) states. Oscillator strength borrowing by CT states has two consequences for the absorption spectrum of PAU_{Me} compared to that for PAAc. First, it reduces the peak oscillator strengths of the $\pi \rightarrow \pi^*$ transitions in PAU_{Me}. Second, it broadens the width of the absorption bands in PAU_{Me} 2–3 fold compared to the corresponding bands in PAAc.

2.2.8. Solvent polarization effects on electronic excited states. Figure 10 illustrates the dramatic effects of equilibrating the solvent to the PAU_{Me} solute with the charge distribution from the first vacuum $P^{\bullet+}/dU^{\bullet-}$ CT state (CT_1). The results illustrated in Figure 10 were obtained for an arbitrary

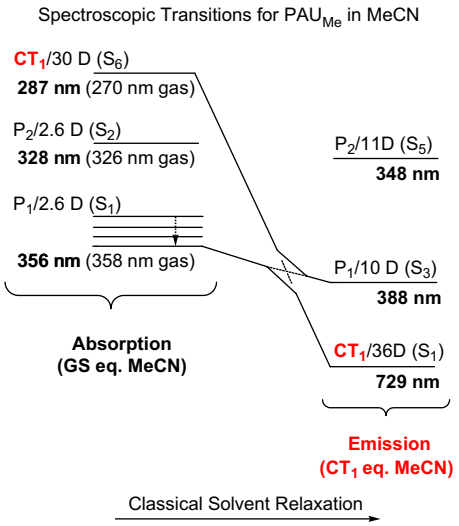

Figure 10. Two electronic transition energy manifolds showing three selected, low energy electronic states (S_n) of a PAU_{Me} conformer in MeCN. (The above data are for conformer E in Mitchell and Netzel.[44] The three configuration defining dihedral angles are the following: (pyrene)C2–C1–N–H(amide)=−44°; H–N–C–O(amide)=157°; and (amide)O–C–C5–C4(uracil)=−130°, where a cis dihedral angle is 0° and clockwise rotations of the nearest bond are negative when facing the rotation axis.) Electronic transitions on the left side of the figure have a selected solvent configuration equilibrated via MD about the charge distribution of the ground state (GS eq. MeCN) producing an 'absorption manifold'; transitions on the right side have a selected solvent configuration equilibrated via MD about the charge distribution of the lowest energy, vacuum CT state (CT_1 eq. MeCN) producing an 'emission manifold'. P_n states correspond to local $^1(\pi,\pi^*)$ excitations of the pyrenyl chromophore. For both the absorption and emission manifolds, separate DRF INDOs/CIS computations yielded the optical transition energies and dipole moment expectation values. For each manifold the illustrated solvent configuration was randomly selected out of 50,000 MD generated solvent configurations using the ground state geometry of conformer E and discrete MeCN molecules both with fixed geometry and atomic charges. Reprinted with permission from the Journal of Physical Chemistry A.[46] Copyright 2006 American Chemical Society.

PAU_{Me} conformer (out of the eight conformers examined in this study) and for two arbitrary solvent configurations, one each for the charge distributions of solute's ground and CT_1 states. For clarity in Figure 10, only three of the lowest energy five or six electronic, excited singlet states are shown for both absorption and emission in MeCN. In particular, the left column of Figure 10 shows the solute's excitation energies (absorption) to three selected excited states and their associated dipole moments for solvent equilibrated about the solute's ground state charge distribution, whereas the right column shows the emission energies and dipole moments of the same three states for solvent equilibrated about the CT_1 state's vacuum charge distribution. Note that the two solvent configurations directly influence the solute's electronic properties via separate DRF INDOs/CIS computations. Thus the solute's excited state emission transitions in the right column closely approximate those of a CT excited state (or photoproduct) 'in a classically relaxed solvent'; however, the solute itself is not relaxed. Rather the PAU_{Me} conformer in the CT_1 state still has the nuclear configuration of the ground state that it had immediately after photoexcitation. This may be not very important, however, because there is no reason to expect that introducing the effects of solute geometry relaxation would yield very different results from those presented here for the particular excited states involved in this study.

Two interesting observations can be made based on Figure 10. One, there is almost no absorption energy difference for the P_1 and P_2 states on going from vacuum to MeCN and only a small difference for CT_1. There likely would be a few more nanometers of red-shift for this vacuum to condensed phase change if dispersion effects were calculated. Two, on going from ground state equilibrated to CT-state equilibrated solvent configurations, the P_1 and P_2 states increase their dipole moments ca. 8 D and their optical transitions red-shift 20–30 nm. The most important result, however, is that for the same change of solvent configuration the CT_1 state's emission energy drops dramatically from 287 nm to 729 nm (2.6 eV!) of which as much as half this drop should be assigned to the up-shifting of the ground state energy in the CT-equilibrated solvent environment. (Whereas INDOs was parameterized appropriately to simulate absorption and emission spectra, its parameters did not provide reliable ground state energies. Consequently, absolute solvation energies for ground states were not calculated in this work.) It is the different charge distributions on the solute in each case that produce the different equilibrated solvent configurations that in turn drive the dramatic differences in the electronic structures of the absorption and emission manifolds of PAU_{Me}.

2.2.9. DRF INDOs/CIS emission spectra for PAAc and PAU_{Me}. Figure 11 presents in the top panel calculated relative emission spectra in MeCN for PAAc and PAU_{Me} using only the lowest energy excited state and in the bottom panel a calculated relative emission spectrum for PAU_{Me} in the same solvent using the two lowest energy excited states along with the experimental emission spectrum of PAdU in MeCN. The top panel shows that the calculated emission maximum of PAAc is at 372 nm compared with an experimental electronic origin of 384 nm both in MeCN. The 12-nm discrepancy is likely due to neglect of dispersion in the DRF INDOs/CIS calculation. The calculated emission maximum of PAU_{Me} is at 359 nm, 13-nm to the blue of that for PAAc. For PAdU the electronic origin of emission is difficult to determine, but may not differ much from that for PAAc. Future work will have to grapple with how to incorporate dispersion effects for excited states into INDO calculations. The heart of this difficulty is that the INDO basis set is not large enough to simulate the diffuseness of excited state wavefunctions.

The bottom panel of Figure 11 shows the calculated CT emission spectrum for PAU_{Me} using transitions from the two lowest energy excited states. In this case, the peak emission intensity increases 7.8-fold and shifts to 345 from 359 nm compared to emission from only the lowest energy excited state shown in the top panel. There are two reasons why emission from PAdU might reasonably be modeled as originating from the two lowest excited states of PAU_{Me}. First, not all pyrenyl $^1(\pi,\pi^*)$ states in PAdU conformers undergo CT quenching within 600 fs. Thus some PAdU conformers emit from their $^1(\pi,\pi^*)$ state much more strongly than from their CT_1 state. Second, the overall shape of the PAdU emission spectrum is closer to that of PAU_{Me} in the bottom panel than in the top panel. In particular in the top panel, the relative intensity of PAU_{Me} emission in the 400–600 nm range is too strong compared to its peak intensity at 359 nm. In the bottom panel, the wider PAdU main

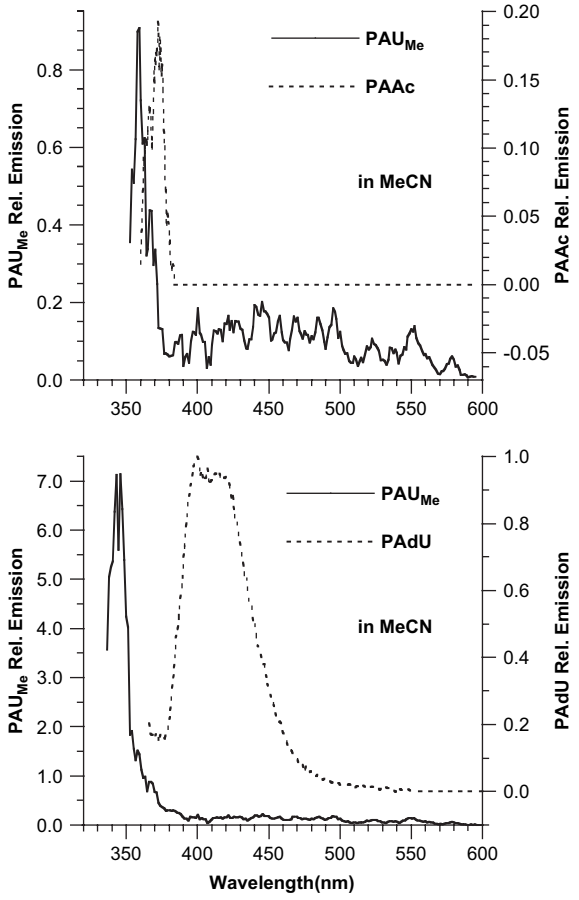

Figure 11. Relative emission spectra in MeCN calculated for both PAU_{Me} and PAAc (top) and calculated for PAU_{Me} and measured for PAdU[29] (bottom). In the figure the calculated spectra for PAU_{Me} and PAAc, respectively, were smoothed over 5- and 2-nm intervals. The calculated emission spectra for PAU_{Me} and PAAc in the top panel were calculated by summing oscillator strengths for the lowest energy excited state over 800 solute/solvent configurations similarly to the summation in Figure 9 but without Boltzmann weighting. As described in Figure 10 for emission spectra, the solvent was equilibrated via MD about the charge distribution of the vacuum CT_1 and P_1 states, respectively, for PAU_{Me} and PAAc. In the bottom panel, the emission spectrum for PAU_{Me} was calculated by summing oscillator strengths for the two lowest energy excited states over 800 solute/solvent configurations. Adapted with permission from the Journal of Physical Chemistry A.[46] Copyright 2006 American Chemical Society.

emission band (54-nm fwhm) compared to the narrower PAU_{Me} main emission band (14-nm fwhm) likely reflects vibronic contributions that are present in the nucleoside but not in the DRF INDOs/CIS computations for PAU_{Me}. The calculated emission spectra for PAU_{Me} in the top and bottom panels of Figure 11 also show that the greatest density of oscillator strength spans approximately 1.11 eV (the 345–500 nm range). Figure 10 shows that thermal solvent fluctuations induce CT_1 emission transitions as far red as 730 nm, but transitions beyond 500 nm make insignificant contributions to emission spectra as they are more than 180-fold less intense than the peak emission intensity near 345 nm.

The DRF INDOs/CIS work on PAU_{Me} models the optical properties of the PAdU nucleoside in polar solvents by calculating the spectral characteristics of a large ensemble of solute/solvent configurations for eight PAU_{Me} conformers in MeCN. It goes beyond an SCRF INDOs/CIS dielectric continuum solvent model by employing explicit MeCN molecules within a discrete reaction field (DRF) solvent model to simulate complete optical band spectra. This approach apart from electrostatic interactions also accounts for many-body polarization interactions and allows for quantitative estimate of the scale of the $P^{\bullet+}/dU^{\bullet-}$ CT state's emission energy variation that thermal solvent fluctuations can produce. Importantly, it also provides richly detailed results on solvent broadening of optical spectra that is especially important for excited states with large dipole moments in polar solvents. Examination of the calculated dipole moments of the excited states produced by light absorption in PAU_{Me} shows that almost all of the large dipole moments ($\geq$25 D) are below 310 nm, i.e., much higher in energy than the lowest energy $^1(\pi,\pi^*)$ state. Thus for the vast majority of PAU_{Me} conformers (and by extension for PAdU also), if MeCN did not fluctuate around their $^1(\pi,\pi^*)$ excited states to lower the energy of their $P^{\bullet+}/dU^{\bullet-}$ CT states, charge transfer would not occur. In fact for a small fraction of PAdU conformers, CT quenching of their pyrenyl $^1(\pi,\pi^*)$ states takes up to 13 ns. However, for a very large fraction of conformers it occurs in less than 600 fs. The remarkable conclusion is that the time of MeCN reorientation—sufficient to allow CT for most PAdU conformers—is $\leq$600 fs.

2.3. Experimental results for ethynyl and ethylenyl linked pyrenyl–dU nucleosides

The above mentioned electronic structure results for PAU_{Me} and $PMAU_{Me}$ show that employing a carbonyl attached to C5 uracil as a linker to join pyrenyl and uracil subunits in pyrenyl–dU nucleoside conjugate makes the energy of the conjugate's $P^{\bullet+}/dU^{\bullet-}$ CT state sensitive to variation of the CO/U_{Me} dihedral angle. Some variation of the Coulombic stabilization energy within CT states among pyrenyl–dU conformers due to variation of the relative separation of their cationic and anionic subunits is unavoidable. However, variation of uracil LUMO delocalization onto linking atoms among nucleoside conformers can be greatly reduced by employing methylenyl, ethylenyl, or ethynyl linkers at the C5 uracil position. Two examples are shown in Figure 12.

2.3.1. PYdU. Figure 13 presents plots of absorption (top) and emission (bottom) spectra for the PYdU nucleoside in deoxygenated MeOH, MeCN, and THF. The top absorption spectra show that the fine structure of the absorption band changes as the solvent is varied. In particular, in the $S_1(0,0)$ region (390–400 nm) PYdU in MeOH has two distinct peaks, in MeCN the higher energy peak becomes a shoulder, and in THF this feature is nearly absent. Similar fine structure changes are also present in the emission

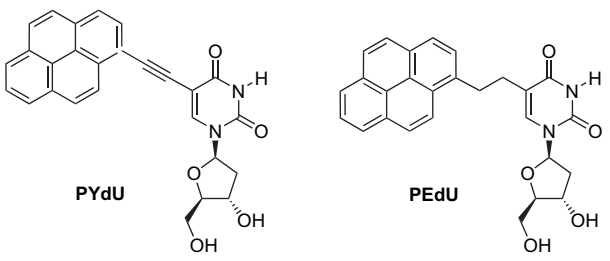

Figure 12. Structural drawings of the PYdU and PEdU pyrenyl–dU nucleoside conjugates.

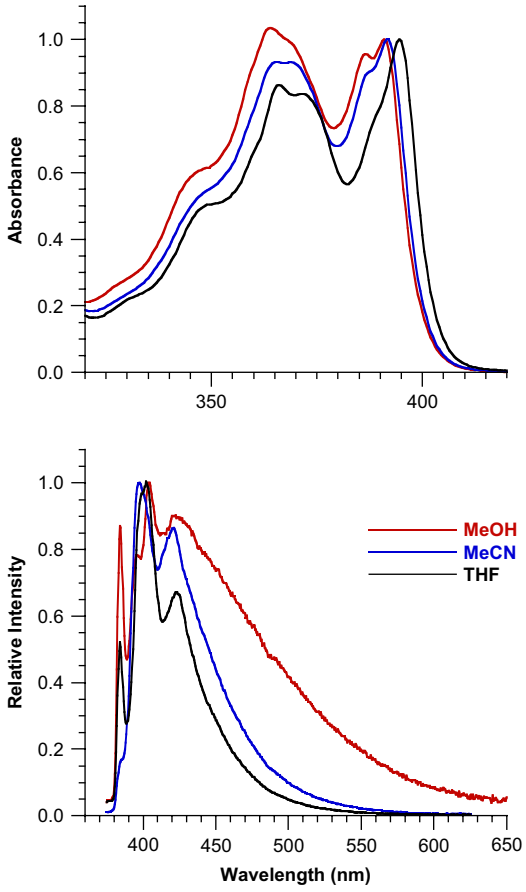

Figure 13. Overlayed plots of absorbance (top) and normalized emission (bottom) spectra for PYdU in the indicated deoxygenated solvents. Absorbance (emission) sample concentrations were, respectively, 1.9×10^{-5} (8.7×10^{-7}), 2.7×10^{-5} (1.3×10^{-6}), and 4.6×10^{-5} M (3.4×10^{-6} M) in MeOH, MeCN, and THF. Molar absorptions (ε) were, respectively, 53.4 (391), 37.5 (392), and 21.5 $mM^{-1}\,cm^{-1}$ (395 nm) in the same solvent series. Adapted with permission from the Journal of Physical Chemistry A.[30] Copyright 2005 American Chemical Society.

spectrum. In particular, in MeOH there are clear features at 384, 396 (small shoulder), 404, and 424 nm; in MeCN the previously strong origin peak at 384 nm is nearly absent and only two peaks at 398 and 423 nm remain with the previous 404 nm peak in MeOH, now only a bulge on the 398 peak; in THF the 384 origin peak is back with clear peaks at 402 and 424 nm with an shoulder at 399 nm. It appears that two sets of correlated emission peaks are present: the very sharp peaks at 384 and 402–404 nm and the broader peaks at 396–398 and 423–424 nm. The principle three peaks (due to C–C vibrations) for 1-ethynylpyrene (PY) are very sharp and occur at 383, 402, and 425 nm in all three solvents. Thus it seems reasonable to assign the sharp two peaks in Figure 13 at 384 and 402–404 nm to 'PY-type' features and the two broader peaks at 396–398 and 423–424 nm to 'PYdU-type' features.

The fact that the intensity of the 384-nm origin peak varies widely as the solvent is changed for the nucleoside but not at all for PY itself, is a strong internal argument that the PY-type peaks in Figure 13 arise from the nucleoside and not from PY impurities. Additionally, the R_f values of PY and PYdU are very different so that separating them is easy. The broader emission peaks at 400 and ca. 424 nm for PYdU in MeOH were reported earlier, but the sharp PY-type peaks were not seen.[67] Presumably the spectral resolution in the earlier study was too low to resolve them. This appears to be the case also in a more recent study of PYdU in MeOH and MeCN.[68] Interestingly, the double peak structure in absorption (Fig. 13 top) for PYdU in MeOH in the $S_1(0,0)$ region (390–400 nm) was seen in both of the other studies. Also, upon change of solvent to dioxane these two peaks were replaced with a single, red-shifted peak as is the case here for change of solvent to THF.[67]

Two important aspects of the emission spectra in Figure 13 (bottom) are that they all have broad, structureless emission extending to long wavelengths and that the relative proportion of their normalized, red emission increases in the solvent series THF, MeCN, and MeOH as solvent changes from nonpolar, to polar, and finally to polar and hydrogen bonding. Such a solvent dependent red-shift of the red emission is expected for emission from a $P^{\bullet+}/dU^{\bullet-}$ CT state. In contrast, the $^1(\pi,\pi^*)$ emission spectrum for PY is nearly invariant within this same solvent series. Relatedly, the emission quantum yield of PYdU decreases in this solvent series as pyrenyl $^1(\pi,\pi^*)$ emission is replaced with CT state emission: 2.1 (THF), 1.5 (MeCN), and 0.47 (MeOH) relative to PBA in deoxygenated MeOH. The emission lifetime in the 450–500 nm range for this CT state in MeOH is 1.06±0.02 ns. Thus, PYdU joins PAdU and PCOdU (τ_{CT}, respectively, 6 and 69 ps in MeOH) as pyrenyl–dU nucleosides with a monoexponential CT state lifetime. The emission spectra in Figure 13 and the measured emission kinetics at eight wavelengths from 383 to 550 nm also make clear that CT emission for PYdU in MeOH extends from 383 to beyond 650 nm, an energy range of more than 1.3 eV that completely overlaps the pyrenyl $^1(\pi,\pi^*)$ emission region.

The single, 1.06-ns lifetime of the CT state of PYdU in MeOH contrasts with the 0.13–38 ns range of lifetimes of this nucleoside's pyrenyl $^1(\pi,\pi^*)$ state seen at 383 and 400 nm. Presumably the wide range of pyrenyl emission lifetimes reflects a wide range of intramolecular CT quenching rates among a variety of PYdU conformers. These widely varying intramolecular ET quenching rates likely reflect electronic coupling differences that in turn have their origin in wavefunction overlap differences between the initial pyrenyl and final CT states of PYdU. In particular, the wavefunction overlap differences for different PYdU conformers may arise mainly from varying phase relationships among the orbitals of the pyrenyl, ethynyl, and dU subunits of the nucleoside as the relative angle of the pyrenyl and dU planes varies among conformers.

2.3.2. Absorption and emission properties of PEdU. Figure 14 presents plots of the absorbance and emission spectra of PEdU and PBA both in MeOH. It is striking how similar the absorptions of these two compounds are in the 300–350 nm pyrenyl S_2 (π,π^*) region. Below 300 nm the absorption of the dU subunit causes the absorption of the nucleoside to exceed that of PBA. Above 350 nm, in the region of the optically forbidden pyrenyl S_1 (π,π^*) state, the nucleoside shows a small amount of increased absorption over that of PBA. In contrast, whereas the absorption of the PEdU nucleoside arises largely from the sum of the absorptions of its two subunits, the emission spectrum of the

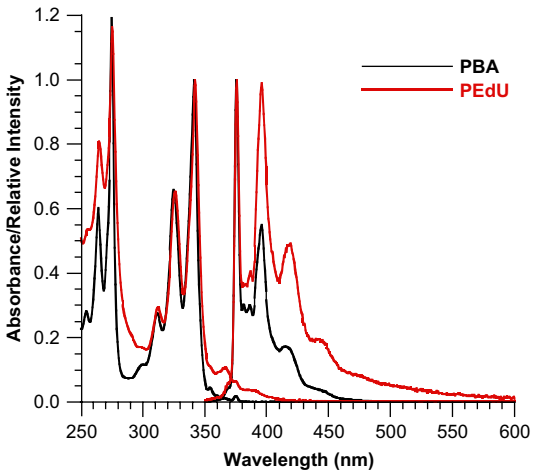

Figure 14. Plots of normalized absorbance and emission spectra for PBA and PEdU in deoxygenated MeOH. The absorbance concentrations were, respectively, 2.4 and 2.3×10^{-5} M for PBA and PEdU in 1-cm path length cells, while emission concentrations were, respectively, 2.9 and 2.2×10^{-6} M also in 1-cm cells. Adapted with permission from the Journal of Physical Chemistry A.[30] Copyright 2005 American Chemical Society.

nucleoside does not look solely like pyrenyl emission. The outstanding difference between the emission spectra for the nucleoside and PBA is that for PBA the emission does not extend significantly beyond 465 nm, while for the nucleoside emission extends beyond 600 nm. Red emission in the 500–600 nm region in pyrenyl–dU nucleosides has previously been identified as arising from the $P^{\bullet+}/dU^{\bullet-}$ CT state.[20,21,29,31,44] Thus in MeOH PEdU exhibits steady state emission features from both the lowest energy $^1(\pi,\pi^*)$ state of its pyrenyl subunit and its $P^{\bullet+}/dU^{\bullet-}$ CT state. The emission quantum yield of PEdU varies dramatically with change of solvent: 0.057 (THF), 0.049 (MeCN), and 0.0072 (MeOH). A seen for other pyrenyl–dU nucleosides, the largest emission quenchings occur in the more polar solvents, MeCN and MeOH. This is expected, because polar solvents lower the energy of highly polar CT states more than less polar (π,π^*) states. The large increase of emission quenching in MeOH versus MeCN again demonstrates that the hydrogen bonding ability of MeOH adds substantial stabilization to the $P^{\bullet+}/dU^{\bullet-}$ CT state in excess of that expected solely from consideration solvent dielectric properties (see above).

In the pyrenyl $^1(\pi,\pi^*)$ emission region from 377 to 450 nm, the fits to PEdU emission kinetics data require four exponential decay lifetimes with the longest lifetime component extending to 78 ns. For example, the average emission lifetime at 396 nm for PEdU in deoxygenated MeOH is 16.4 ns: 0.61 ns (0.49), 5.2 ns (0.24), 13.8 ns (0.09), and 76 ns (0.18). In the CT region from 500 to 550 nm, three exponential lifetimes are sufficient to fit the kinetics data, and the longest lifetime is 10 ns. For example, the average CT emission lifetime at 550 nm in the same solvent is 2.4 ns: 0.78 ns (0.45), 2.63 ns (0.45), and 8.6 ns (0.10). The presence of dioxygen shortens the average pyrenyl $^1(\pi,\pi^*)$ emission lifetime to 3.2 ns at 396 nm, but has negligible effect on the average CT emission lifetime. For O_2 to quench pyrenyl $^1(\pi,\pi^*)$ emission in less than 25 ns in aerated MeOH, the quenching reaction must occur within PEdU·O_2 complexes formed in the ground state prior to photoexcitation. Note that a dioxygen concentration of 10^{-3} M times a bimolecular quenching rate of $10^{10}\,M^{-1}\,s^{-1}$ would yield a diffusional quenching time of ca. 100 ns.

2.3.3. Picosecond TA spectroscopy of PEdU in MeOH.

Figure 15 presents plots of TA spectra for PBA and PEdU in aerated MeOH at 25 ps after photoexcitation (top) and of picosecond TA kinetics for PEdU at 710 nm (bottom). The presence of dioxygen reduces emission; nevertheless TA measurements still could not be made below 460 nm due to emission interference. The TA spectrum of PBA shows an absorption maximum at 470 nm and a small shoulder at 510 nm. These features agree reasonably with a previously reported absorption maximum at 490 nm and a broad shoulder in the 510–520 nm region for the pyrenyl $^1(\pi,\pi^*)$ state of BPT in dimethyl formamide solution.[15] Similarly, the $^1(\pi,\pi^*)$ TA spectrum of pyrene in *n*-octane at 60 ps after excitation has a prominent broad peak at 459 nm, a weaker broad peak at 501 nm, and a weak absorption band around

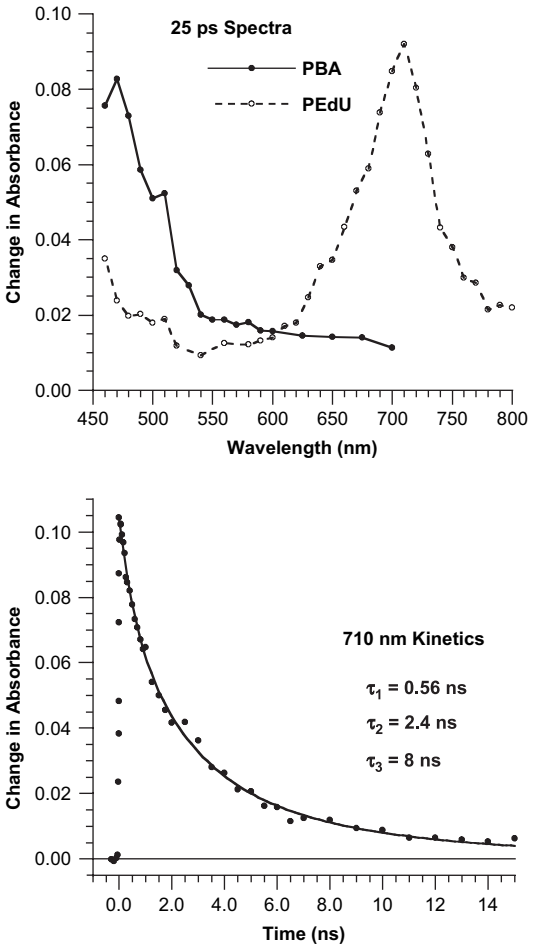

Figure 15. Picosecond TA (ΔA) spectral plots (top) for PBA and PEdU in aerated MeOH at 25 ps after photoexcitation and a picosecond TA kinetics plot (bottom) for PEdU in deoxygenated MeOH at 710 nm: 2.0×10^{-4} M PBA and 1.0×10^{-4} M PEdU. The TA kinetics at 710 nm were fit with a triexponential function without deconvolution of the laser system's instrument response: $\Delta A(t)=m1\exp(-t/\tau_1)+m2\exp(-t/\tau_2)+m3\exp(-t/\tau_3)$. The fit parameters were: $m1=0.025\pm0.013$, $m2=0.054\pm0.010$, $m3=0.025\pm0.005$, $\tau_1=0.56\pm0.24$ ns, $\tau_2=2.4\pm0.7$ ns, and $\tau_3=8\pm1.5$ ns. The R value for the fit was 0.998. Fits to a biexponential function also with a constant term equal to zero did not give uniformly distributed residuals. Adapted with permission from the Journal of Physical Chemistry A.[30] Copyright 2005 American Chemical Society.

560 nm.[69] Approximately 30% of the initial TA of PBA at 470 nm decays during the 15-ns time window of the experiment (data not shown). This small amount of TA relaxation is consistent with a pyrenyl $^1(\pi,\pi^*)$ lifetime of 20–45 ns assuming, respectively, small to negligible formation of a pyrenyl $^3(\pi,\pi^*)$ state in aerated MeOH (an asymptote). For PEdU in aerated MeOH, approximately 70% of the initial TA signal at 470 nm decays during the 15-ns TA time window (data also not shown). This TA decay is consistent with a monoexponential lifetime of 2.4–9.0 ns assuming, respectively, larger to smaller asymptotes. This range of TA lifetimes agrees with the 2.4–3.7 ns (0.2–0.6 amplitude) pyrenyl emission decay components in the 377–450 nm range observed for PEdU in aerated MeOH. Consequently part of the TA kinetics of PEdU in aerated MeOH in the 460–530 nm range is consistent with relaxation of the pyrenyl $^1(\pi,\pi^*)$ state.

In contrast to the TA spectrum of PBA in Figure 15, the TA absorbance spectrum of PEdU has a moderate absorption increase at 460 nm, no maximum at 470 nm, and a strikingly strong absorption maximum at 710 nm. An earlier study by Shafirovich and Geacintov et al.[15] of the BPT cation, formed by two-photon excitation of BPT at 355 nm, shows a narrow pyrenyl cation absorption band at 460 nm ($\varepsilon_{max}=3.0\times10^4$ M^{-1} cm^{-1}) and weak featureless absorption beyond 525 nm. Clearly at 25 ps after photoexcitation, PEdU's TA spectrum is not assignable exclusively to the lowest energy pyrenyl $^1(\pi,\pi^*)$ state as it is in PBA. Furthermore, the absorption decrease from 460 nm to 540 nm for PEdU is not consistent with the spectrum of the lowest energy pyrenyl $^3(\pi,\pi^*)$ state, which absorbs strongly at 420 nm and weakly beyond 440 nm but with a moderate absorption increase from 475 to 525 nm.[15] Thus together, the 460-nm absorption increase for PEdU in Figure 15, the strong emission quenching in MeOH for PEdU relative to PBA (91%), and the red CT product emission in the 500–600 nm region in Figure 14, argue that the TA spectrum for PEdU in Figure 15 recorded 25 ps after excitation is due mainly to the $P^{\bullet+}/dU^{\bullet-}$ CT state.

The bottom plot in Figure 15 shows that the TA signal at 710 nm for PEdU in deoxygenated MeOH has an excitation-pulse-limited rise time (formation in $\leq$30 ps) and decays with triexponential lifetimes of 0.56±0.24, 2.4±0.7, and 8±1.5 ns. (Note that a least squares fit of the 710-nm TA data to a biexponential function also with a constant term equal to zero, does not give uniformly distributed residuals). Crucially, the TA lifetimes in Figure 15 accord with the average CT emission lifetimes in deoxygenated MeOH in the 500–550 nm range: 0.80±0.06, 2.7±0.15, and 9.4±1.2 ns. Figure 15 shows that the full width at half maximum (fwhm) of the 710-nm absorption band of PEdU is ca. 70 nm. Thus the absorption band at 710 nm for PEdU in MeOH is too narrow, too short lived,[15] and appears to be too strongly absorbing to arise from solvated electrons. Additional studies of 710-nm absorption strength versus excitation energy (linear, not quadratic), kinetics in the presence and absence of dioxygen (no change), kinetics at various wavelengths of the 710-nm band (the same), and kinetics versus sample concentration (no change) leave little doubt that this 710-nm band is due to the $P^{\bullet+}/dU^{\bullet-}$ CT state. A striking result reported by Fiebig and co-workers is that PYdU (to be discussed next) has a strong 700-nm TA band in MeOH that is almost identical to the 710-nm TA band of PEdU also in MeOH in Figure 15.[68]

2.3.4. Nanosecond TA Spectroscopy of PEdU in MeOH. Figure 16 presents plots of a TA spectrum at 400 ns (top) and nanosecond TA kinetics at 420 nm (bottom) for PEdU in aerated MeOH. A striking observation in the top spectrum is the presence of TA increases expected for the pyrenyl T_1 (π,π^*) state at 416 and 512 nm on either side of the TA band at 462 nm due to $P^{\bullet+}$. (It is worth noting here that only $P^{\bullet+}$ absorption without accompanying T_1 state TA bands was seen 347 ns after photoexcitation of PEdU in deoxygenated MeOH.) The bottom plot shows that at 420 nm the pyrenyl $^1(\pi,\pi^*)$ emission (−TA) decays with an apparent lifetime of 9 ns; this corresponds to the formation time of the T_1

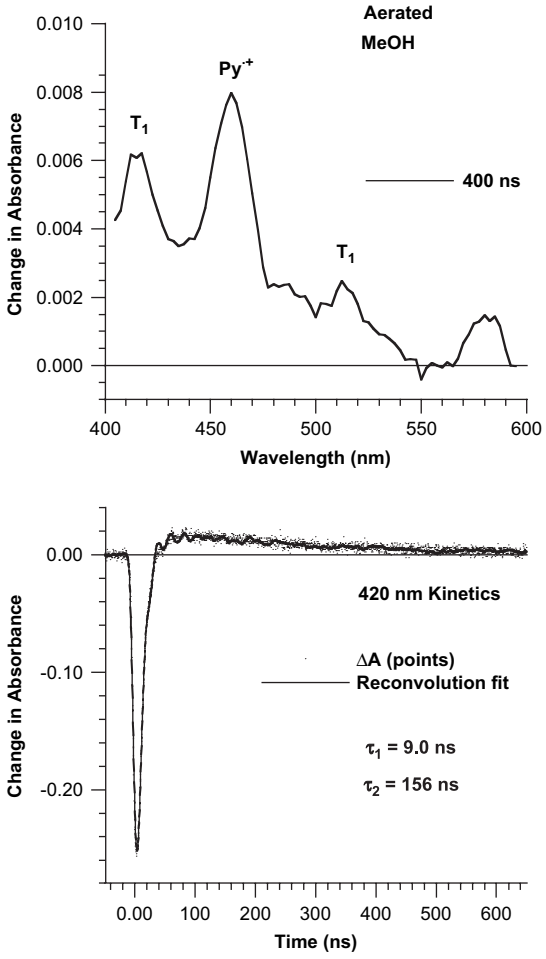

Figure 16. Spectral (top) and kinetics (bottom) plots of nanosecond TA data (ΔA) for 8×10^{-6} M PEdU in aerated MeOH photoexcited with a 6-ns duration laser pulse at 341-nm. TA measurements were made in static sample cells with 1-cm path lengths using a 4-mm diameter excitation beam at 90° with respect to the probe beam. (A_{341} in a 1-cm path length cell was 0.34.) In the top plot, the time window for the gated CCD detector was 200 ns and centered 400 ns after excitation. The spectrum has 80 data points taken every 2.5 nm and was smoothed over 10-nm spectral intervals. In the bottom plot, the kinetics data (corresponding to pyrenyl S_1 state emission (−TA) and T_1 state absorbance (+TA)) were recorded at 420 nm with 1.8-nm spectral resolution. Lifetimes were obtained from iterative reconvolution fits of the TA data to instrument response convoluted biexponential functions. The fit lifetimes were 9.0±1.5 ns (rinse) and 156±12 ns (decay) with an asymptote of 0.001. Adapted with permission from the Journal of Physical Chemistry A.[30] Copyright 2005 American Chemical Society.

state's TA increase. Eventually, the T_1 state decays with lifetime of 156 ns. Also for PEdU in aerated MeOH, nanosecond TA data at 462 nm show that pyrenyl $^1(\pi,\pi^*)$ emission decays with an apparent lifetime of 3 ns but that the T_1 state's decay lifetime (163 ns) is the same within error as at 420 nm. The different pyrenyl $^1(\pi,\pi^*)$ TA decay lifetimes at 420 nm (9 ns) and 462 nm (3 ns) agree with average lifetimes from emission kinetics, respectively, at 416 nm (11 ns) and 475 nm (3 ns). Aerating the MeOH solution of PEdU formed PEdU·O_2 adducts that statically quenched the pyrenyl $^1(\pi,\pi^*)$ state. Some of this $^1(\pi,\pi^*)$ quenching yielded T_1 state products; some of it also produced long-lived $P^{\bullet+}$ products (and presumably also corresponding $O_2^{\bullet-}$ products). A clear result was that at 462 nm the TA decreased as the T_1 state decayed (data not shown). If the decay of the T_1 state had yielded long-lived $P^{\bullet+}$ products, the 462-nm absorbance would have increased. It did not; thus in PEdU·O_2 adducts only the pyrenyl $^1(\pi,\pi^*)$ and not the $^3(\pi,\pi^*)$ state reacted to form long-lived $P^{\bullet+}$ products.

The overall conclusions of the nanosecond TA studies of PEdU in MeOH are that static oxidative quenching of the pyrenyl $^1(\pi,\pi^*)$ state by dioxygen to form small amounts of pyrenyl cation occurs even in solutions of PEdU in MeOH that are deoxygenated by bubbling with nitrogen gas. Surprisingly, aerating the PEdU solutions does not significantly increase the yield of pyrenyl cation, but does increase the rate of intersystem crossing from the pyrenyl $^1(\pi,\pi^*)$ to the $^3(\pi,\pi^*)$ state, and the T_1 state becomes observable in TA studies. The T_1 state, however, does not form a $^3(Py^{\bullet+}/dU^{\bullet-})$ CT state most likely because this reaction is moderately endothermic. Saturating the PEdU solution with O_2 actually decreases the yield of pyrenyl cation due to increasing about 3-fold the rate of the pyrenyl $^1(\pi,\pi^*)$ state to $^3(\pi,\pi^*)$ state intersystem crossing apparently without increasing significantly the rate of oxidative quenching of the pyrenyl $^1(\pi,\pi^*)$ state by dioxygen (assuming cage escape yields of $Py^{\bullet+}$ and $O_2^{\bullet-}$ products are independent of oxygenation state of MeOH). Increasing the concentration of O_2 in MeOH solutions with PEdU by aeration and O_2 bubbling not only increases the yield of the pyrenyl T_1 (π,π^*) state but also shortens its lifetime: $\tau(T_1)$, respectively, 160 and 36 ns in aerated and O_2-saturated MeOH. As noted, the pyrenyl $^3(\pi,\pi^*)$ state is not oxidatively quenched by O_2 within PEdU·O_2 adducts; however, this is not for thermodynamic reasons, because O_2 is easy to reduce $(E_{1/2}(O_2/O_2^{\bullet-})=-0.56$ V (SHE)).[70] Perhaps formation of the $^3(\pi,\pi^*)$ state within PEdU·O_2 adducts is accompanied by dissociation of bound O_2. If so, $^3(\pi,\pi^*)$ state oxidative quenching by O_2 would be diffusion controlled and dependent on the concentration of dissolved dioxygen.

Independent of the presence or absence of dioxygen (including both aeration and O_2-saturation of MeOH), $P^{\bullet+}/dU^{\bullet-}$ CT state formation is excitation-pulse limited and its decay lifetime is constant within error, ca. 2.5 ns.

The rich detail of excited state relaxations described above can be summarized as shown in Figure 17. Two populations of PEdU photoexcited nucleosides (S_1) are present, those bound to O_2 (Fig. 17a) and those free of O_2 (Fig. 17b); each decays via different relaxation pathways. For PEdU·O_2 (S_1) adducts, there is competition between charge separation to form $P^{\bullet+}$ and $O_2^{\bullet-}$ and intersystem crossing to form the T_1 state (presumably also accompanied by dissociation of O_2). For such nucleosides, the S_1 state does not form the $P^{\bullet+}/dU^{\bullet-}$ CT state as both the T_1 state and $P^{\bullet+}/O_2^{\bullet-}$ photoproducts are lower in energy. Whereas the T_1 state has enough energy to form $P^{\bullet+}$ and $O_2^{\bullet-}$ products, it reacts only with free O_2 at diffusion controlled rates (note τ (T_1) is, respectively, 160 and 36 ns in aerated and O_2-saturated MeOH). For nucleosides free of O_2, the S_1 state forms the CT state with a variety of lifetimes depending on the relative conformation of the PEdU subunits; in most conformers intramolecular CT occurs in $\leq$30 ps. The CT state relaxes to S_0 with lifetimes ranging from $\approx$1 to 10 ns without forming the T_1 state indicating that for it charge recombination is faster than intersystem crossing.

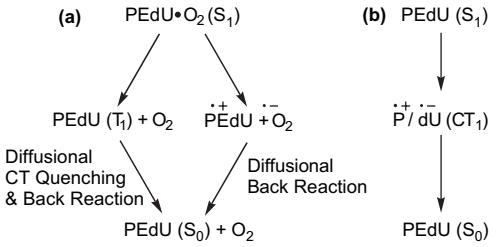

Figure 17. Summary of excited state relaxations for PEdU in MeOH, where S_1 refers to the lowest energy pyrenyl $^1(\pi,\pi^*)$ state, T_1 to the pyrenyl $^3(\pi,\pi^*)$ state, CT_1 to the $P^{\bullet+}/dU^{\bullet-}$ charge transfer state, and S_0 to the ground state. The lifetime of the T_1 state is shortened due to diffusion controlled, oxidative quenching by dioxygen followed back reaction of the separated charges. Presumably the lifetime of most separated charges is short compared to the quenching time; thus an increase in $P^{\bullet+}/dU+O_2^{\bullet-}$ products is not observed as the T_1 state decays.

2.3.5. Pyrenyl–dU nucleoside structures and CT state lifetimes. Importantly, the ratio of the CT state's energy $(E(CT_1)=-\Delta G^0_{CR})$ to the charge recombination (CR) reorganization energy (λ) determines how 'inverted' the $P^{\bullet+}/dU^{\bullet-}$ charge recombination reaction is.[34–38] Other factors being equal, a more rigid nucleoside will have a lower CT reorganization energy than one with a more flexible structure. Additionally, a nucleoside with more extended subunits will have a higher CT_1 state energy (less Coulombic stabilization) than one with closer subunits. Earlier we discussed that PAdU, PCOdU, PYdU form a series of pyrenyl–dU nucleosides with monoexponential CT state lifetimes, respectively, 6 ps, 69 ps, and 1.06 ns. Not unrelatedly, all of these nucleosides have reasonably fixtured pyrenyl and uracil subunits, and the energy of their CT_1 states increases within this series with PAdU having the lowest energy CT_1 state and PYdU the highest one. Thus the pattern of increasing CT_1 state lifetime on going from PAdU to PYdU likely results from progressively more inverted charge recombination reactions in this series of nucleosides.

PdU, PMAdU, and PEdU have lowest energy $P^{\bullet+}/dU^{\bullet-}$ CT states with multiple lifetimes whose averages in MeOH are, respectively, 0.54 ns, 2.1 ns, and 2.5 ns. Differences in charge recombination reorganization energy, electronic coupling, and free energy among conformer subpopulations are responsible for the different charge recombination dynamics shown by each of these nucleosides. Among the six nucleosides just mentioned, PMAdU, PEdU, and PYdU show the greatest promise for forming high yields of long-lived, photoinduced charge separation products in DNA duplexes in

which they are substituted. Substitution of PYdU along with an electron-acceptor labeled nucleoside into DNA may work, but the pyrenyl ligands in PMAdU and PEdU need to be prevented from contacting reactive DNA bases, including the uracil subunits to which they are attached. Surrounding pyrenyl–dU nucleotides within DNA duplexes by redox-inactive labels (such as phenyl or pyridinyl groups) attached to neighboring nucleotide bases might be able to 'cage' pyrenyl groups and channel their CT reactions. In this spirit, it would be instructive to cage the pyrenyl subunit of PEdU in a DNA duplex and to see how long its $P^{\bullet+}/dU^{\bullet-}$ CT state would live. However, constructing pyrenyl–dU labeled DNA with a caged pyrenyl group is complicated and might not be necessary if excess electron transfer was fast enough from the uracil anion in a $P^{\bullet+}/dU^{\bullet-}$ CT state to a nearby electron-acceptor labeled nucleotide. The next two DNA studies to be discussed, one using PEdU[71] and the other PYdU[72] substitution, were directed at finding out how facile excess electron transfer was to nearby 5-XdU traps, where X=Br or F.

2.4. Experimental results for PEdU and PYdU substituted DNA

2.4.1. PEdU substituted DNA. At the start of this discussion, it is important to point out that a number of studies have shown that excess electrons can travel in DNA from source to trap sites.[73–85] To date, however, only low yields of long-lived, charge separated photoproducts have been reported in this area. Thus the challenge of forming high yields of long-lived, charge separated photoproducts in DNA based on photoinduced excess electron transfer remains. Achieving this goal will likely make practical a number of applications in DNA in sensing, medical diagnostics assays, and even molecular electronics. Important success in forming long-lived (hundred of microseconds), charge separated photoproducts in DNA based on photoinduced hole transfer has recently been achieved, but substantial uncertainty remains regarding the quantum yield of these long-lived photoproducts.[86–92] Another unresolved question regarding hole transfer in DNA concerns the intriguing possibility that the formation of solvent stabilized polarons with a length of approximately four bases may play a crucial role in determining the yield of long-lived CT products when four or more AT pairs separate the hole injection and trapping sites.[2]

Nine DNA hairpins (HPs) were studied at room temperature to observe their $P^{\bullet+}/dU^{\bullet-}$ CT excited state dynamics following photoexcitation at 355 nm with a 25-ps laser pulse.[71] The HPs were 18–24 bases long, had a central tetra-T loop, and had a single U^{PE} (PEdU nucleoside) substitution in the central region of their stems. Three of the HPs were also substituted with 5-XdU traps (U^X) to learn about the effects of these traps on CT excited state lifetimes and emission quantum yields in U^{PE}-substituted HPs. Table 5 lists the base sequences of the nine U^{PE} substituted HPs, and Figure 18 presents a molecular model of HP **8**.

The HPs in Table 5 fall into two main groups: those containing U^F and U^{Br} excess electron traps (**6–8**) and those lacking electron traps (**1–5** and **9**). The emission quantum yield data in Table 5 show that the lowest emission quantum yields ($0.14–0.27\times10^{-2}$) belong to HPs **1–3** and **9** that lack traps,

Table 5. DNA hairpin base sequence and emission quantum yield (ϕ_{em})

HP	Base sequence[a]	ϕ_{em} ($\times10^2$)[b]
1	TTU^{PE}TTG TTTT AAAAAAA	0.16
2	CTTU^{PE}TTG TTTT AAAAAAG	0.23
3	GTTU^{PE}TTG TTTT AAAAAAC	0.14
4	TTTTTTU^{PE}AAG TTTT CTTAAAAAAA	0.40
5	GAAU^{PE}AAG TTTT ATTATTC	0.75
6	CT$U^F U^{PE}$AAG TTTT CTTAAAG	1.04
7	CT$U^F U^{Br} U^{PE}$AAG TTTT CTTAAAAG	0.64
8	C$U^F U^{Br}$TTU^{PE}AAG TTTT CTTAAAAAG	1.21
9	TTTU^{PE}TTG TTTT AAAAAAA	0.27

[a] 5′→3′ Base sequence. Data obtained from Ref. 71.
[b] Emission quantum yields were measured relative to PBA in deaerated MeOH with ϕ_{em} equal to 0.065.[20] ϕ_{em} errors are ±10%.

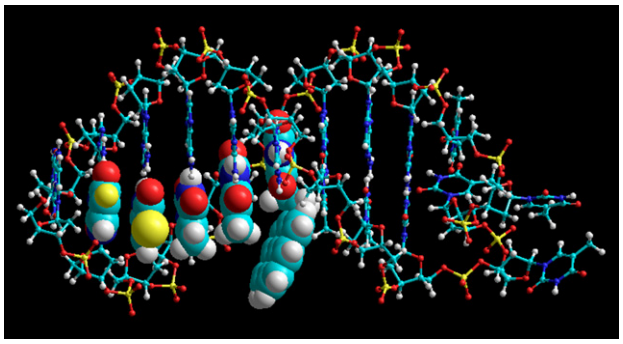

Figure 18. A molecular mechanics model of HP **8** built with HyperChem 7.51 using the Amber99 force field.[98] The backbone and base pairs in the stem were constrained to B-form DNA geometry, while all modifications at C5 uracil positions and the tetra-T loop were simultaneously geometry optimized. (Other energy-minimized conformations with different pyrenyl and loop geometries also exist.) In place of explicit solvent and counter ions, a distance-dependent dielectric constant of 78 was used with no cutoff for nonbonded interactions. In the chart the tetra-T loop is on the right, and HP **8**′s stem is on the left. Five same-strand uracils in the stem are shown as overlapping spheres of van der Waals radius, 5′-$U^F U^{Br}$TTU^{PE}-3′; their C5-substituents, respectively, F, Br, Me, Me, and ethylenylpyrenyl are turned toward the reader. The rest of HP **8** is displayed as a balls-and-cylinders rendering. Reprinted with permission from the Journal of Physical Chemistry B.[71] Copyright 2005 American Chemical Society.

while larger emission quantum yields ($0.64–1.21\times10^{-2}$) belong to HPs **6–8** that contain traps. HPs **4** and **5** have intermediate emission quantum yields, respectively, 0.40 and 0.75×10^{-2}, but their emission spectra differ from those of the other seven HPs in that they have significantly more pyrenyl $^1(\pi,\pi^*)$ emission. The emission spectra can be separated into two distinct groups. The first group contains HPs **1–3** and **6–9** as all seven have only hints of pyrenyl $^1(\pi,\pi^*)$ emission features at 376, 396, and 422 nm. Rather their spectra are almost entirely due to $P^{\bullet+}/dU^{\bullet-}$ CT emission from the U^{PE} nucleotide. This CT emission maximizes around 450 nm and extends beyond 600 nm far to the red of the pyrenyl emission. As expected for such emission, it is structureless due to strong coupling between the nuclear motions of the polar CT excited state and the buffer solution. Importantly, measurement of the CT emission kinetics to the red of the pyrenyl emission range allows direct observation of the lifetime of the $P^{\bullet+}/dU^{\bullet-}$ CT state within U^{PE}.

By considering the set of six HPs lacking U^X electron traps (**1–5** and **9**), a pattern of emission spectral-type and quantum yield can be seen. HPs **1–3** have two or three Ts flanking U^{PE} on the same stem-strand on both sides. They also have low

emission quantum yields ($0.14–0.23\times10^{-2}$) and CT emission band shapes with essentially complete quenching of pyrenyl $^1(\pi,\pi^*)$ emission. HP **4** in contrast has six Ts flanking U^{PE} on the same stem-strand in the 5′-direction, but no same stem-strand pyrimidines in the 3′-direction. It has both a higher emission quantum yield (0.40×10^{-2}) than HPs **1–3** and a large amount of pyrenyl $^1(\pi,\pi^*)$ emission. Clearly HPs **1–3** quench pyrenyl $^1(\pi,\pi^*)$ emission more effectively than does HP **4**. HP **5** confirms this explanation. HP **5** has no same stem-strand pyrimidines on either side of U^{PE}, and it has both a large amount of pyrenyl $^1(\pi,\pi^*)$ emission and the largest emission quantum yield of all six duplexes that lack U^X traps, 0.75×10^{-2}. Thus there is a pattern of increased emission quantum yield and lessening of pyrenyl $^1(\pi,\pi^*)$ emission quenching as same stem-strand pyrimidines flanking U^{PE} are reduced from pyrimidines on both sides, to pyrimidines on only the 5′-side, to no pyrimidines on either side of U^{PE}.

Detailed emission quantum yield comparisons among the nine HPs that also take into account differences in average CT lifetime are revealing. (Average emission lifetimes conveniently condense the information in the triexponential CT emission kinetics observed for all nine HPs.) HPs **1–3** have no traps and an average CT emission lifetime (measured at 525 nm in the center of the CT region) of 1.03±0.16 ns; their average CT emission quantum yield is $0.18\pm0.05\times10^{-2}$. However, HPs **6** and **7** with U^X traps adjacent to U^{PE} have an average CT emission lifetime of 2.09±0.15 ns and an average CT emission quantum yield of $0.84\pm0.20\times10^{-2}$. Thus while the average CT lifetime increased 2-fold for the two HPs with traps compared to HPs **1–3**, their emission quantum yields increased even more, three to five times. Admittedly positioning electron traps immediately adjacent to U^{PE} is not likely to be the best strategy for producing the long-lived CS products. Thus the lifetime and quantum yield results for HP **8** with two Ts separating the U^{Br} trap and U^{PE} are particularly significant. HPs **8** and **9** have similar average CT lifetimes, respectively, 2.52 and 2.30 ns (both ±0.20 ns). However, HP **9** lacking an electron trap has an emission quantum yield of only 0.27×10^{-2}, while HP **8** has a yield of 1.21×10^{-2}, a 4.5-fold increase. Thus compared to HPs lacking traps, it is reasonable to conclude that HPs with electron traps in the 5′-direction on the same strand as U^{PE} show enhanced CT emission quantum yields in excess of those expected based on comparison with average CT emission lifetimes.

The fact that HPs **1–5** lacking U^X traps show an average CT lifetime of 1.06±0.15 ns indicates good reproducibility for this measurement whether same-strand Ts adjacent to the U^{PE} electron source are present in both the 5′- and 3′-directions, present only in the 5′-direction, or even absent in both directions. (In this context, the 2.30-ns average CT lifetime of HP **9** is anomalous.) In contrast to HPs **1–5** and **9**, however, all three HPs (**6–8**) with U^X electron traps on the same strand as U^{PE} have both an average CT lifetime in the 2.1–2.5 ns range and enhanced CT emission quantum yield (i.e., in excess of that expected based on relative CT lifetimes). The combination of these two differences for HPs **6–8** compared to all six other HPs strongly suggests that direct electron injection from pyrenyl $^1(\pi,\pi^*)$ states to U^X sites is occurring in U^{PE} substituted HPs in addition to formation of the $P^{\bullet+}/dU^{\bullet-}$ CT state within U^{PE} itself. This conclusion is further supported by the increase in pyrenyl $^1(\pi,\pi^*)$ emission features and in total emission quantum yield that is seen as same-strand Ts flanking U^{PE} are switched to the opposite strand (see HPs **4** and **5** compared to HPs **1–3** in Table 5). The increased CT emission quantum yield in HPs **6–8** compared to HPs **1–3** likely results from directly injected electrons on $U^{X\bullet-}$ migrating to uracil in $U^{PE\bullet+}$ (i.e., $P^{\bullet+}dU$) and thus indirectly forming the emissive $P^{\bullet+}dU^{\bullet-}$ CT state of U^{PE}. This latter conclusion appears reasonable as excess electron hopping toward $U^{PE\bullet+}$ is favored by Coulombic attraction.

Some observations that were not found in this work are important also. HPs **2** and **3** differed from HP **1** in that they had 5′-terminal dC and dG nucleotides, respectively. If dC were a good electron trap either as $dC^{\bullet-}$ or as $dC(H)^{\bullet}$ on either the same or opposite strand as U^{PE}, one would have expected to see lifetime lengthening of the $P^{\bullet+}dU^{\bullet-}$ CT state of U^{PE} as trapped electrons on dC would have been delayed in returning to $U^{PE\bullet+}$ relative to the case in HP **1**. No such lifetime lengthening was seen in the CT emission of HPs **2** and **3** compared to **1**. Relatedly, if excess electrons readily hopped via dT sites away from $U^{PE\bullet+}$, for HP **4** they would have been delayed in returning to $U^{PE\bullet+}$ relative to their return times in HPs **1–3** because there were six dTs on the 5′-side of U^{PE} in HP **4** compared to two–three in HPs **1–3**. No such lifetime lengthening was seen in the CT emission of HP **4** compared to HPs **1–3**. Indeed the average CT lifetime of HPs **1–3** was 1.03±0.16 ns, while that of HP **4** was 0.99 ns. Clearly moving excess electrons from the $P^{\bullet+}dU^{\bullet-}$ CT state of U^{PE} away from $U^{PE\bullet+}$ to isoenergetic trapping sites such as dT and dC or to shallow traps such as U^X was not favorable. High yields of long-lived charge separated photoproducts based on initial formation of a $P^{\bullet+}dU^{\bullet-}$ CT are still possible, but three conditions would likely have to be met to accomplish this: (1) a deep electron trap should be used; (2) the lifetime of the $P^{\bullet+}dU^{\bullet-}$ CT state should be sufficiently long (likely $\geq$1 ns); and (3) the reduced trap ($trap^{\bullet-}$) and $U^{PE\bullet+}$ should be kept separated from each other.

2.4.2. PYdU substituted DNA. To test the above conclusions, a second work studied six DNA duplexes substituted with U^{PY} (PYdU nucleoside) at 10 °C to observe their $P^{\bullet+}/dU^{\bullet-}$ CT excited state dynamics following photoexcitation at 355 nm.[72] All were 13 base pairs long and had a central ethynylpyrenyl U^{PY} nucleotide. Importantly, four of these duplexes were also substituted near U^{PY} in the 5′-direction with a same-strand U^F nucleotide to serve as an excess electron trap. (See Table 6 for DNA duplex base sequences.)

Table 6. DNA duplex base sequence, emission quantum yield (ϕ_{em}), and average CT lifetime ($<\tau>$)

Duplex	Base sequence[a]	ϕ_{em}[b]	$<\tau>$, ns
D1	GGTTTTU^F*U*^{PY}AAAGG	0.020	1.14
D2	GGTTTU^{F}TU^{PY}AAAGG	0.016	1.13
D3	GGTTU^{F}TTU^{PY}AAAGG	0.022	1.23
D4	GGTU^{F}TTTU^{PY}AAAGG	0.021	1.37
D5	GGATAA*U*^{PY}AATAGG	0.017	1.22
D6	GGAATT*U*^{PY}TTAAGG	0.032	1.48

[a] 5′→3′ Base sequence. Data obtained from Ref. 72.
[b] Emission quantum yields were measured relative to PBA in deaerated MeOH with Φ_{em} equal to 0.065.[20] ϕ_{em} errors are ±10%.

Some idea of the relative effect on uracil reduction potential due to changing a C5 uracil methyl to a fluoro group can be estimated by noting that in the case of flavin mononucleotide (FMN) the $2e^-$ reduction potential of FMN_{ox}/1,5-dihydro-$FMN_{red}H_2$ varies due to substitution at position 8 as −208 (Me), −167 (F), and −148 (Br) versus the standard hydrogen electrode.[93] Thus U^F and U^{Br} nucleotides are likely to be 40–50 mV easier to reduce than T. In agreement with these considerations, the work by Gaballah et al.[71] showed that 5′-adjacent U^F and U^{Br} traps were more effective oxidative quenchers of the local pyrenyl $^1(\pi,\pi^*)$ state of U^{PE} than a 5′-adjacent T. Additionally, both U^F and U^{Br} were shown to be shallow electron traps as excess electrons on them migrated to $U^{PE\bullet+}$ to form the emissive $P^{\bullet+}dU^{\bullet-}$ CT state of U^{PE}. Because the ethynyl linker in U^{PY} is more rigid than the ethylenyl linker in U^{PE}, most if not all direct injection of electrons to U^X sites found in the first study should be eliminated in the U^{PY}-substituted duplexes. Additionally, if the excess electron in the $P^{\bullet+}/dU^{\bullet-}$ CT product of U^{PY} is restrained from hopping to nearby U^F traps due to attraction to $P^{\bullet+}$, the CT emission quantum yield and average lifetime of U^{PY}-substituted duplexes should be independent of trap presence and location.

The emission spectral shapes for duplexes **D1**–**D5** are identical to each other with maxima at 448 nm. The emission spectrum of **D6**, however, is red-shifted with a maximum at 464 nm. All emission spectra for duplexes **D1**–**D6** are very similar to that for PYdU in MeOH in Figure 13 with the difference that the sharp 'PY-type' peaks are missing. Both the absorbance and emission spectra of **D6** indicate that the local environment surrounding the pyrenyl chromophore in U^{PY} is somewhat different than those of the other five duplexes. The base sequence of **D6** is unique among the six duplexes in that it has a pair of same-strand Ts flanking U^{PY} in the 3′-direction, while all five other duplexes have a pair of As in this position. This change in 3′-bases flanking U^{PY} appears to be responsible for the modest changes in absorbance and emission spectra for **D6** compared to the other five duplexes. Table 6 also presents emission quantum yields for the six duplexes in this study. Importantly, duplexes **D1**–**D5** have the same emission quantum yield, 0.019±0.003. **D6** again is modestly different with a higher emission quantum yield than the other five duplexes, 0.032.

Table 6 shows that duplexes **D1**–**D5** have an average CT lifetime of 1.22 (σ ±0.10) ns; that is, their average CT lifetimes are the same independent of where the U^F trap is located or even whether or not a U^F trap is present. This result also accords with the finding that duplexes **D1**–**D5** have the same emission quantum yield. **D6** has both a higher emission quantum yield (0.032) and a higher average CT lifetime (1.48 ns) than duplexes **D1**–**D5**. However, within error, the quantum yield increase is consistent with the average CT emission lifetime increase. Thus the CT lifetime and emission quantum yield data for duplexes **D1**–**D6** are in accord.

U^{PY}-substituted duplexes, where enhanced CT emission quantum yield (i.e., a quantum yield above that expected due to increased average CT lifetime) is lacking for duplexes with U^F electron traps compared to duplexes without traps, contrast strongly with U^{PE}-substituted HPs where up to 4.5-fold enhanced CT emission quantum yield is found for HPs with U^{Br} and U^F traps compared to HPs without traps.[71] The first paper ascribed the enhanced CT emission quantum yield in the presence of U^X electron traps to direct injection of electrons to U^X sites from the pyrenyl excited state of U^{PE} to form $P^{\bullet+}/U^{X\bullet-}$ products that subsequently decayed to form the emissive $P^{\bullet+}/dU^{\bullet-}$ CT state of U^{PE}. Key to this pyrenyl oxidative quenching process was the flexible ethylenyl linker in U^{PE}. The observation for U^{PY}-substituted duplexes that there is no enhancement of CT emission quantum yield when U^F electron traps are located near U^{PY} supports the earlier HP work, because the rigid ethynyl linker in U^{PY} is not expected to permit pyrenyl oxidative quenching by such traps.

The rigidity of PYdU has also been exploited as a sensitive fluorescence probe to discriminate between fully complementary duplexes and ones with a single mismatched base opposite PYdU. For example, the relative fluorescence for a duplex with dA opposite PYdU was 5.6 times stronger than the one with dT opposite PYdU.[94] Similarly, both PYdU and PYdA (8-(1-ethynylpyrenyl)-2′-deoxyadenosine) have been used to probe the B-to-Z duplex transition that can be induced on going from low salt to high salt concentrations.[95] For both ethynylpyrenyl nucleosides each attached without a complementary base to the end of a 9-mer of alternating dGdC sequences, the B-form of duplex was more stable than the Z-form due to either PYdU or PYdA end-stacking. The result was that the labeled duplexes produced much less emission in low salt than in high salt, respectively, from $P^{\bullet+}/dU^{\bullet-}$ and $P^{\bullet-}/dA^{\bullet+}$ CT states. Finally, a molecular beacon was also formed by substituting PYdG (8-(1-ethynylpyrenyl)-2′-deoxyguanosine) and PYdC (5-(1-ethynylpyreny)-2′-deoxycytidine) as a base pair in the stem of the beacon.[96,97] Without the presence of DNA complementary to the beacon, the beacon emitted largely from PYdG. With the addition of DNA complementary to the beacon, the PYdG·PYdC base pair dissociated, and energy transfer from photoexcited PYdC to PYdG was disrupted. This produced strong emission from PYdC in the 400–450 nm region.

3. Conclusion

The conclusion is straightforward. Continued systematic study of pyrenyl–dU substituted DNA duplexes will be able to achieve high yields of long-lived, photoinduced charge separated photoproducts. (Using other types of labeled nucleotides to reach the some goal is not precluded.) However, to accomplish this goal, judicious use of complementary strategies will likely be required. One was discussed earlier. Surrounding pyrenyl–dU nucleotides within DNA duplexes by redox-inactive labels (or blockers such as phenyl or pyridinyl groups) attached to neighboring nucleotide bases to 'cage' the pyrenyl groups and channel their CT reactions. One or two carefully placed blocking groups using an appropriate linker will probably suffice. Another strategy is to use deep rather than shallow electron traps, perhaps more than one in a cascade of progressively deeper traps at increasing distances from pyrenyl–dU. Keeping $P^{\bullet+}/trap^{\bullet-}$ products separate from each other would lengthen their lifetime and could be facilitated by locating a redox-inactive blocker between them. Finally, an auxiliary electron-donor (D) labeled nucleotide could be substituted near $U^{P\bullet+}$ to

reduce it in competition with $P^{\bullet+}/dU^{\bullet-}$ or $P^{\bullet+}/trap^{\bullet-}$ charge recombination. The combined use of a deep trap (or cascade of traps) and an auxiliary donor is very likely to produce a high yield of a long-lived $D^{\bullet+}/trap^{\bullet-}$ product in DNA following photoexcitation of a pyrenyl–dU nucleotide conjugate.

Acknowledgements

I thank Professor Nicholas Geacintov for helpful discussions and encouragement over many years, my senior collaborators Professors Bruce E. Eaton, Tianquan (Tim) Lian, Lucjan Strekowski, Piet van Duijnen, and Drs. Morteza Vaghefi, Larry Morrison, and Ken Cruickshank for crucial assistance and exciting interactions, and my students and postdocs C. Denise Mitchell, Galen Collier, Dr. Samir Gaballah, Dr. Yasser Hussein, Dr. Joshua Telser, and Dr. Charles Kerr for their conscientious, enthusiastic, and diligent laboratory work. I also thank Marla Netzel for valuable literature research assistance. It has been a pleasure and an honor to have worked with each of these individuals.

References and notes

1. Ren, W.; Wang, J.; Ma, Z.; Guo, H. *Phys. Rev. B* **2005**, *72*, 0354561–0354565.
2. Conwell, E. M. *Proc. Natl. Acad. Sci. U.S.A.* **2005**, *102*, 8795–8799.
3. Siriwong, K. *A Combined Quantum Mechanics and Molecular Dynamics Study of Charge Transfer in DNA*; Doktors der Naturwissenschaften, Technischen Universität München: München, 2004; p 136.
4. Lewis, F. D.; Zhang, L.; Liu, X.; Zuo, X.; Tiede, D. M.; Long, H.; Schatz, G. C. *J. Am. Chem. Soc.* **2005**, *127*, 14445–14453.
5. Voityuk, A. A. *J. Phys. Chem. B* **2005**, *109*, 10793–10796.
6. Telser, J.; Cruickshank, K. A.; Morrison, L. E.; Netzel, T. L. *J. Am. Chem. Soc.* **1989**, *111*, 6966–6976.
7. Dreyer, G. B.; Dervan, P. B. *Proc. Natl. Acad. Sci. U.S.A.* **1985**, *82*, 968–972.
8. Gillam, I. C.; Tener, G. M. *Anal. Biochem.* **1986**, *157*, 199–207.
9. Helene, C.; Toulme, F.; Delarue, M.; Asseline, U.; Takasugi, M.; Maurizot, M.; Montenay-Garestier, T.; Thuong, N. T. *Oligodeoxynucleotides Covalently Linked to an Intercalating Agent, Structural and Thermodynamic Studies of a Dodecathymidylate and its Binding to Polynucleotides*; Sarma, R. H., Sarma, M. H., Eds.; Adenine: New York, NY, 1986; pp 119–130.
10. Telser, J.; Cruickshank, K. A.; Schanze, K. S.; Netzel, T. L. *J. Am. Chem. Soc.* **1989**, *111*, 7221–7226.
11. Kumar, C. V.; Barton, J. K.; Turro, N. J. *J. Am. Chem. Soc.* **1985**, *107*, 5518–5523.
12. Telser, J.; Cruickshank, K. A.; Morrison, L. E.; Chan, C.-K.; Netzel, T. L. *J. Am. Chem. Soc.* **1989**, *111*, 7226–7232.
13. Mann, J. S.; Shibata, Y.; Meehan, T. *Bioconjugate Chem.* **1992**, *3*, 554–558.
14. Margulis, L.; Pluzhnikov, P. F.; Mao, B.; Kuzmin, V. A.; Chang, Y. J.; Scott, T. W.; Geacintov, N. E. *Chem. Phys. Lett.* **1991**, *187*, 597–603.
15. Shafirovich, V. Y.; Levin, P. P.; Kuzmin, V. A.; Thorgeirsson, T. E.; Kliger, D. S.; Geacintov, N. E. *J. Am. Chem. Soc.* **1994**, *116*, 63–72.
16. Shafirovich, V. Y.; Courtney, S. H.; Ya, N.; Geacintov, N. E. *J. Am. Chem. Soc.* **1995**, *117*, 4920–4929.
17. O'Connor, D.; Shafirovich, V. Y.; Geacintov, N. E. *J. Phys. Chem.* **1994**, *98*, 9831–9839.
18. Valis, L.; Mayer-Enthart, E.; Wagenknecht, H.-A. *Bioorg. Med. Chem. Lett.* **2006**, *16*, 3184–3187.
19. Manoharan, M.; Tivel, K. L.; Zhao, M.; Nafisi, K.; Netzel, T. L. *J. Phys. Chem.* **1995**, *99*, 17461–17472.
20. Netzel, T. L.; Zhao, M.; Nafisi, K.; Headrick, J.; Sigman, M. S.; Eaton, B. E. *J. Am. Chem. Soc.* **1995**, *117*, 9119–9128.
21. Netzel, T. L.; Nafisi, K.; Headrick, J.; Eaton, B. E. *J. Phys. Chem.* **1995**, *99*, 17948–17955.
22. Raytchev, M.; Mayer, E.; Amann, N.; Wagenknecht, H.-A.; Fiebig, T. *ChemPhysChem* **2004**, *5*, 706–712.
23. Kaden, P.; Mayer-Enthart, E.; Trifonov, A.; Fiebig, T.; Wagenknecht, H.-A. *Angew. Chem., Int. Ed.* **2005**, *44*, 1636–1639.
24. Mayer-Enthart, E.; Wagenknecht, H.-A. *Angew. Chem. Int. Ed.* **2006**, *45*, 3372–3375.
25. Yamana, K.; Ohashi, Y.; Nunota, K.; Kitamura, M.; Makano, H.; Sangen, O.; Shimidzu, T. *Tetrahedron Lett.* **1991**, *32*, 6347–6350.
26. Yamana, K.; Iwase, R.; Furutani, S.; Tsuchida, H.; Zako, H.; Yamaoka, T.; Murakami, A. *Nucleic Acids Res.* **1999**, *27*, 2387–2392.
27. Nakamura, M.; Fukunaga, Y.; Sasa, K.; Ohtoshi, Y.; Kanaori, K.; Hayashi, H.; Nakano, H.; Yamana, K. *Nucleic Acids Res.* **2005**, *33*, 5887–5895.
28. Nakamura, M.; Yamana, K. *Chem. Commun.* **2005**, 5163–5165.
29. Kerr, C. E.; Mitchell, C. D.; Headrick, J.; Eaton, B. E.; Netzel, T. L. *J. Phys. Chem. B* **2000**, *104*, 1637–1650.
30. Gaballah, S.; Hussein, Y. H. A.; Anderson, N.; Lian, T. T.; Netzel, T. L. *J. Phys. Chem. A* **2005**, *109*, 10832–10845.
31. Kerr, C. E.; Mitchell, C. D.; Ying, Y.-M.; Eaton, B. E.; Netzel, T. L. *J. Phys. Chem. B* **2000**, *104*, 2166–2175.
32. Steenken, S. *Free Radical Res. Commun.* **1992**, *16*, 349–379.
33. Trifonov, A.; Buchvarov, I.; Wagenknecht, H.-A.; Fiebig, T. *Chem. Phys. Lett.* **2005**, *409*, 277–280.
34. Sutin, N. *Nuclear and Electronic Factors in Electron Transfer: Distance Dependence of Electron-Transfer Rates*; Bolton, J. R., Mataga, N., McLendon, G., Eds.; Advances in Chemistry Series; American Chemical Society: Washington, DC, 1991; Vol. 228, pp 25–43.
35. Marcus, R. A.; Sutin, N. *Biochim. Biophys. Acta* **1985**, *811*, 265–322.
36. Brunschwig, B.; Sutin, N. *Comments Inorg. Chem.* **1987**, *6*, 209–235.
37. Brunschwig, B. S.; Ehernson, S.; Sutin, N. *J. Phys. Chem.* **1987**, *91*, 4714–4723.
38. Sutin, N.; Creutz, C. *J. Chem. Educ.* **1983**, *60*, 809–814.
39. Marcus, R. A. *J. Chem. Phys.* **1956**, *24*, 966–978.
40. Marcus, R. A.; Siders, P. *J. Phys. Chem.* **1982**, *86*, 622–630.
41. Siders, P.; Marcus, R. A. *J. Am. Chem. Soc.* **1981**, *103*, 748–752.
42. DeVault, D. *Q. Rev. Biophys.* **1980**, *13*, 387–564.
43. Sutin, N.; Brunschwig, B. *Some Aspects of Electron Transfer in Biological Systems*; Johnson, M. K., King, R. B., Kurtz, D. M., Kutal, C., Norton, M. L., Scott, R. A., Eds.; Advances in Chemistry Series; American Chemical Society: Washington, DC, 1990; Vol. 226, pp 65–88.
44. Mitchell, C. D.; Netzel, T. L. *J. Phys. Chem. B* **2000**, *104*, 125–136.

45. Onsager, L. *J. Am. Chem. Soc.* **1936**, *58*, 1486–1493.
46. Duijnen, P. T. v.; Netzel, T. L. *J. Phys. Chem. A* **2006**, *110*, 2204–2213.
47. Ridley, J. E.; Zerner, M. C. *Theor. Chim. Acta* **1973**, *32*, 111–134.
48. Koopmans, v. T. *Physica* **1934**, *1*, 104–113.
49. Zerner, M. C. *Semi Empircal Molecular Orbital Methods*; Lipkowitz, K. B., Boyd, D. B., Eds.; VCH: New York, NY, 1991; Vol. 2, pp 313–366.
50. Zerner, M. C.; Loew, G. H.; Kirchner, R. F.; Mueller-Westerhoff, U. T. *J. Am. Chem. Soc.* **1980**, *102*, 589–599.
51. Karelson, M. M.; Zerner, M. C. *J. Phys. Chem.* **1992**, *96*, 6949–6957.
52. Thole, B. T.; Duijnen, P. T. v. *Theor. Chim. Acta* **1980**, *55*, 307–318.
53. Thole, B. T.; Duijnen, P. T v *Chem. Phys.* **1982**, *71*, 211–220.
54. Vries, A. H. d.; Duijnen, P. T. v.; Juffer, A. H.; Rullmann, J. A. C.; Dijkman, J. P.; Merenga, H.; Thole, B. T. *J. Comput. Chem.* **1995**, *16*, 37–55.
55. Duijnen, P. T. v.; Grozema, F. C.; Swart, M. *J. Mol. Struct. (THEOCHEM)* **1999**, *464*, 191–198.
56. Thole, B. T.; Duijnen, P. T. v. *Theor. Chim. Acta* **1983**, *63*, 209–221.
57. Swart, M.; Duijnen, P. T. v.; Snijders, J. G. *J. Comput. Chem.* **2001**, *22*, 79–88.
58. Thole, B. T. *Chem. Phys.* **1981**, *59*, 341–350.
59. Duijnen, P. T. v.; Swart, M. *J. Phys. Chem. A* **1998**, *102*, 2399–2407.
60. Swart, M.; Duijnen, P. T. v.; Snijders, J. G. *J. Mol. Struct. (THEOCHEM)* **1999**, *458*, 11–17.
61. Ridley, J. E.; Zerner, M. C. *Theor. Chim. Acta* **1979**, *42*, 223–236.
62. Baerends, E. J. *Amsterdam Density Functional*; Vrje Universiteit: Amsterdam, 2007. http://www.scm.com.
63. Jensen, L.; Åstrand, P.-O.; Osted, A.; Kongsted, J.; Mikkelson, K. V. *J. Chem. Phys.* **2002**, *116*, 4001–4010.
64. Toxvaerd, T. *Mol. Phys.* **1991**, *72*, 159–168.
65. Swart, M.; Duijnen, P. T. v. *Mol. Simul.* **2006**, *32*, 471–484.
66. Coutinho, K.; Oliveira, M. J. D.; Canuto, S. *Int. J. Quantum Chem.* **1998**, *66*, 249–253.
67. Korshun, V. A.; Manasova, E. V.; Balakin, K. V.; Prokhorenko, I. A.; Buchatskii, A. G.; Berlin, Y. A. *Russ. J. Bioorg. Chem.* **1996**, *22*, 807–809.
68. Trifonov, A.; Raytchev, M.; Buchvarov, I.; Rist, M.; Barbaric, J.; Wagenknecht, H.-A.; Fiebig, T. *J. Phys. Chem. B* **2005**, *109*, 19490–19495.
69. Foggi, P.; Pettini, L.; Santa, I.; Righini, R.; Califano, S. *J. Phys. Chem.* **1995**, *99*, 7439–7445.
70. Atkins, P.; de Paula, J. *Physical Chemistry*; W.H. Freeman: New York, NY, 2002; p 1092.
71. Gaballah, S. T.; Vaught, J. D.; Eaton, B. E.; Netzel, T. L. *J. Phys. Chem. B* **2005**, *109*, 5927–5934.
72. Gaballah, S. T.; Collier, G.; Netzel, T. L. *J. Phys. Chem. B* **2005**, *109*, 12175–12181.
73. Breeger, S.; Hennecke, U.; Carell, T. *J. Am. Chem. Soc.* **2004**, *126*, 1302–1303.
74. Behrens, C.; Carell, T. *Chem. Commun.* **2003**, 1632–1633.
75. Behrens, C.; Ober, M.; Carell, T. *Eur. J. Org. Chem.* **2002**, 3281–3289.
76. Behrens, C.; Cichon, M. K.; Grolle, F.; Hennecke, U.; Carell, T. Excess Electron Transfer in Defined Donor-Nucleobase and Donor-DNA-Acceptor Systems. *Topics in Current Chemistry*; Schuster, G. B., Ed.; Springer: Berlin, 2004; Vol. 236, pp 187–204.
77. Giese, B.; Carl, B.; Carl, T.; Carell, T.; Behrens, C.; Hennecke, U.; Shiemann, O.; Feresin, E. *Angew. Chem.* **2004**, *116*, 1884–1887.
78. Haas, C.; Kraling, K.; Cichon, M. K.; Rahe, N.; Carell, T. *Angew. Chem.* **2004**, *116*, 1878–1880.
79. Manetto, A.; Breeger, S.; Chatgilialoglu, C.; Carell, T. *Angew. Chem., Int. Ed.* **2006**, *45*, 318–321.
80. Shafirovich, V. Y.; Dourandin, A.; Luneva, N. P.; Geacintov, N. E. *J. Phys. Chem.* **1997**, *101B*, 5863–5868.
81. Messer, A.; Carpenter, K.; Forzley, K.; Buchanan, J.; Yang, S.; Razskazovskii, Y.; Cai, Z.; Sevilla, M. D. *J. Phys. Chem. B* **2000**, *104*, 1128–1136.
82. Cai, Z.; Xifeng, L.; Sevilla, M. D. *J. Phys. Chem. B* **2002**, *106*, 2755–2762.
83. Chatterjee, M.; Rokita, S. E. *J. Am. Chem. Soc.* **1990**, *112*, 6397–6399.
84. Ito, T.; Rokita, S. E. *J. Am. Chem. Soc.* **2003**, *125*, 11480–11481.
85. Ito, T.; Rokita, S. E. *Angew. Chem., Int. Ed.* **2004**, *43*, 1839–1842.
86. Takada, T.; Kawai, K.; Fujitsuka, M.; Majima, T. *Angew. Chem., Int. Ed.* **2006**, *45*, 120–122.
87. Kawai, K.; Takada, T.; Tojo, S.; Majima, T. *J. Am. Chem. Soc.* **2003**, *125*, 6842–6843.
88. Takada, T.; Kawai, K.; Fujitsuka, M.; Majima, T. *Proc. Natl. Acad. Sci. U.S.A.* **2004**, *101*, 14002–14006.
89. Takada, T.; Kawai, K.; Cai, X.; Sugimoto, A.; Fujitsuka, M.; Majima, T. *J. Am. Chem. Soc.* **2004**, *126*, 1125–1129.
90. Lewis, F. D.; Liu, X.; Miller, S. E.; Hayes, R. T.; Wasielewski, M. R. *J. Am. Chem. Soc.* **2002**, *124*, 14020–14026.
91. Lewis, F. D.; Liu, X.; Miller, S. E.; Wasielewski, M. R. *J. Am. Chem. Soc.* **1999**, *121*, 9746–9747.
92. Lewis, F. D.; Zhu, H.; Daublain, P.; Fiebig, T.; Raytchev, M.; Wang, Q.; Shafirovich, V. *J. Am. Chem. Soc.* **2006**, *128*, 791–800.
93. Eckstein, J. W.; Hastings, J. W.; Ghisla, S. *Biochemistry* **1993**, *32*, 404–411.
94. Hwang, G. T.; Seo, Y. J.; Kim, S. J.; Kim, B. H. *Tetrahedron Lett.* **2004**, *45*, 3543–3546.
95. Seo, Y. J.; Kim, B. H. *Chem. Commun.* **2005**, 150–152.
96. Wagner, C.; Rist, M.; Mayer-Enthart, E.; Wagenknecht, H.-A. *Org. Biomol. Chem.* **2005**, *3*, 2062–2063.
97. Mayer, E.; Valis, L.; Wagner, C.; Rist, M.; Amann, N.; Wagenknecht, H.-A. *ChemBioChem* **2004**, *5*, 865–868.
98. *HyperChem Professional, Beta 1 Release 7.51 for Windows*; Hypercube: Gainesville, FL, 2003.
99. Amann, N.; Pandurski, E.; Fiebig, T.; Wagenknecht, H.-A. *Angew. Chem., Int. Ed.* **2002**, *41*, 2978–2980.
100. Amann, N.; Pandurski, E.; Fiebig, T.; Wagenknecht, H.-A. *Chem.—Eur. J.* **2002**, *8*, 4877–4883.